Mineralium Deposita (2023) 58:1351–1370
https://doi.org/10.1007/s00126-023-01181-z

ARTICLE

Lithium enrichment in the Salar de Diablillos, Argentina, and the influence of Cenozoic volcanism in a basin dominated by Paleozoic basement

Carisa Sarchi[1,2] · Friedrich Lucassen[2] · Anette Meixner[2] · Pablo J. Caffe[1] · Raúl Becchio[3] · Simone A. Kasemann[2]

Received: 13 December 2022 / Accepted: 16 May 2023 / Published online: 22 June 2023

Abstract
Salars with lithium-rich brines are a characteristic feature of the Central Andes, but knowledge about the main sources of lithium and the mobilization processes of lithium in the salar deposits is still incomplete. This work focuses especially on the Salar de Diablillos (southern Puna) as part of a larger area that includes the neighboring Salar Centenario and Salar de Ratones. Building on the ability of Li as a tracer of silicate weathering, we investigate the Li content and isotope composition of samples from the depocenter and catchment of the Diablillos basin (3-D) and conduct a surface reconnaissance in the Centenario and Ratones depocenters to identify the key metallogenic processes. Radiogenic Sr and Nd isotope compositions are also provided to discriminate the main local Li sources. The isotope data in all three depocenters show that most of the Li in the brines and evaporite deposits are derived from Cenozoic volcanic rocks, despite the dominance of the Paleozoic basement in the catchment. In the Centenario and Ratones depocenters, near-surface chemical weathering appears to be the dominant Li mobilization process. In contrast, hydrothermal mobilization of Li also plays a role in the Salar de Diablillos, possibly related to the presence of a fractured basement with pressure zones and artesian conditions in the aquifer at depth. These fluids also show a larger element contribution from the basement.

Keywords Lithium isotopes · Salar deposits · Puna · Lithium triangle · Central Andes

Introduction

The Altiplano-Puna plateau of the Central Andes is considered the largest continental plateau related to subduction in the world. It forms an extensive morphostructure (1800 km long and 400 km wide) with an average elevation of 3700 m a.s.l. (Isacks 1988; Allmendinger et al. 1997; Prezzi et al. 2009). It is characterized by numerous endorheic basins (hereafter "closed basins") bounded by north–south oriented mountain ranges (Turner 1970; Vandervoort et al. 1995). Their depositional center (depocenters) host silicate detritus from the restricted catchment areas and commonly evaporite deposits in salt lakes and salt pans, also known as salars, in their morphological deepest sections (Risacher et al. 2003). The evaporite deposits formed under long-term, generally arid climatic conditions (Strecker et al. 2007), and many of them host world-class brine pool deposits of lithium (Li) (López Steinmetz 2017; López Steinmetz and Salvi 2021). At present, the world's largest lithium reserves in brines are geographically confined to the SW Bolivia–NW Argentina–NE Chile segment of the plateau (between about 20° and 27° S), an area informally referred to as the "Lithium Triangle" (Grosjean et al. 2012).

The current transition to a low-carbon society has triggered an ever-increasing demand of Li for high energy density batteries, e.g., in electric vehicles (Goodenough 2016). Lithium has become a new in-demand element, and the lithium-rush is pushing the Central Andean salar deposits

Editorial handling: B. Lehmann

✉ Carisa Sarchi
csarchi@idgym.unju.edu.ar

[1] Instituto de Ecorregiones Andinas (INECOA–Universidad Nacional de Jujuy–CONICET) and Instituto de Geología y Minería (Universidad Nacional de Jujuy), Av. Bolivia 1661, (CP:4600) S.S. de Jujuy, Argentina

[2] Faculty of Geosciences and MARUM-Center for Marine Environmental Sciences, University of Bremen, Leobener Str. 8, 28359 Bremen, Germany

[3] Instituto de Bio y Geociencias del NOA, (IBIGEO–Universidad Nacional de Salta–CONICET), Av. Bolivia 5150, (CP:4000), Salta, Argentina

into the spotlight. Despite conceptual models of the genesis of Li brine deposits (e.g., Munk et al. 2016), detailed case studies of Li sources and the generation of Li-rich brines in individual Andean salar deposits are still rare. Munk et al. (2016) presented a list of six characteristics that continental Li-rich salar deposits have in common, including: (1) arid climate; (2) closed basin containing a salar, a salt lake, or both; (3) associated igneous and/or hydrothermal activity; (4) tectonically driven subsidence; (5) suitable Li sources; and (6) sufficient time to concentrate Li. Of these, the source of Li is probably the most discussed topic, together with the processes involved in mobilizing Li from the primary source rocks and concentrating in salt pans.

Generally, two main lithological groups are proposed as the primary sources of Li in the Central Andes: (1) the Cenozoic felsic volcanic rocks, especially the large intermediate and silicic ignimbrite rocks (Alonso et al. 1991; Risacher and Fritz 2009; Hofstra et al. 2013; Orberger et al. 2015; García et al. 2020; Meixner et al. 2020, 2021; Chen et al. 2020; Muller et al. 2020, among others) and (2) the Paleozoic (Pz) metamorphic-magmatic-sedimentary basement rocks (Meixner et al. 2020; López Steinmetz et al. 2020) that recycle older, Proterozoic, continental material (Bahlburg and Berndt 2016; Büttner et al. 2005; Willner et al. 2008). Activation of Li from these sources is known to occur via low-temperature weathering processes and/or hydrothermal leaching (Godfrey et al. 2013; Godfrey and Álvarez-Amado 2020; Risacher et al. 2003, 2011; Peralta Arnold et al. 2017; López Steinmetz 2017; García et al. 2020; Marazuela et al. 2020; Franco et al. 2020; Meixner et al. 2021). Other factors that might also contribute to Li enrichment of brines include recycling of Li-rich clays (Godfrey and Álvarez-Amado 2020; López Steinmetz et al. 2018) and remobilization of buried Li-rich salts (Marazuela et al. 2020). However, these cannot be considered as primary lithium sources, but rather as intermediate reservoirs where Li was previously concentrated after its primary mobilization from Li-rich source rocks, as described above.

Li isotopes are useful tracers for identifying and distinguishing low-temperature weathering processes from higher-temperature hydrothermal processes, especially in silicate rocks (Pogge von Strandmann et al. 2020 and references therein), while radiogenic Sr isotopes are useful tracers of source rocks in sedimentary systems and host rocks in freshwater surveys (Palmer and Edmond 1989). The combination of both isotope systems is a promising tool for evaluating Li cycling in closed basins, assuming that the clastic sedimentary infill ("clastic" in the following) represents eroded material from catchment areas and that water enters the system mainly via surface runoff and groundwater flow.

Studies using both Li and Sr isotope systems to determine the sources of clastic infill and water supply to the Li-bearing basins are still limited (Munk et al. 2018; Godfrey et al. 2019; Godfrey and Álvarez-Amado 2020; García et al. 2020; Meixner et al. 2021). In the southern Puna, where the study area is located (Fig. 1), comprehensive studies have been conducted on Salar de Hombre Muerto (Godfrey et al. 2013) and Salar de Pozuelos (Meixner et al. 2021). An exploratory study was conducted on Salar de Centenario and Ratones (Orberger et al. 2015), but it did not include Sr isotope data. A regional assessment of the Li and Sr isotopic composition of the Pz-basement and Cenozoic volcanic rocks of the Central Andes as potential source rocks was recently published by Meixner et al. (2020).

To further our understanding of the different processes of Li mobilization (weathering and/or hydrothermal leaching) and accumulation that play an important role in the salars of the southern Puna in north-western Argentina, this work focuses on the Centenario (CN), Ratones (RT), and Diablillos (Di) basins, that host the smallest salars that are among the world-class brine deposits in the Lithium-Triangle. We use Sr and Nd isotopes for source tracing and Li contents and Li isotopes to constrain Li mobilization from source to deposition. Materials studied include catchment and basin surface samples of the salars and samples from wells and cores (to a depth of 250 m) from the Salar de Diablillos.

Geological setting of the research area

The Argentine Puna is located south of 22° S (Fig. 1) and is characterized by the development of internally drained tectonic depressions with active evaporite accumulation, limited by uplifted blocks (bounded by reverse faults) (Turner 1970; Vandervoort et al. 1995). The surface geology of the Puna is dominated by young volcanic rocks, with extensive ignimbrite sheets especially in the northern Puna, and mafic to intermediate volcanic centers in the south. Magmatic, low-grade metamorphic, and sedimentary rocks of Early Paleozoic age form the oldest basement, cropping out north of the Calama-Olacapato-Toro lineament (Fig. 1). In the southern Puna, the Lower Pz-basement occurs alongside with Ediacaran to Early Cambrian metasedimentary rocks (Hongn and Seggiaro 2001; Rapela et al. 2018). Metamorphism of the basement varies from low- to high-grade (Mon and Hongn 1987; 1996; Büttner et al. 2005).

The study area is located in the southern Puna (Fig. 1) in an elongated intermontane depression, NNE-SSW oriented, and includes three closed drainage (hydrographical) basins, each with defined catchment areas. From N to S, these are the Centenario (CN), Ratones (RT), and Diablillos (Di) basins (Figs. 2 and 3). Due to the arid climate, the hydrological balance of the closed basins is negative, and evaporation exceeds the relatively small discharges of fluvial tributaries. These conditions lead to the formation of brines enriched in various easily soluble metals such as lithium and

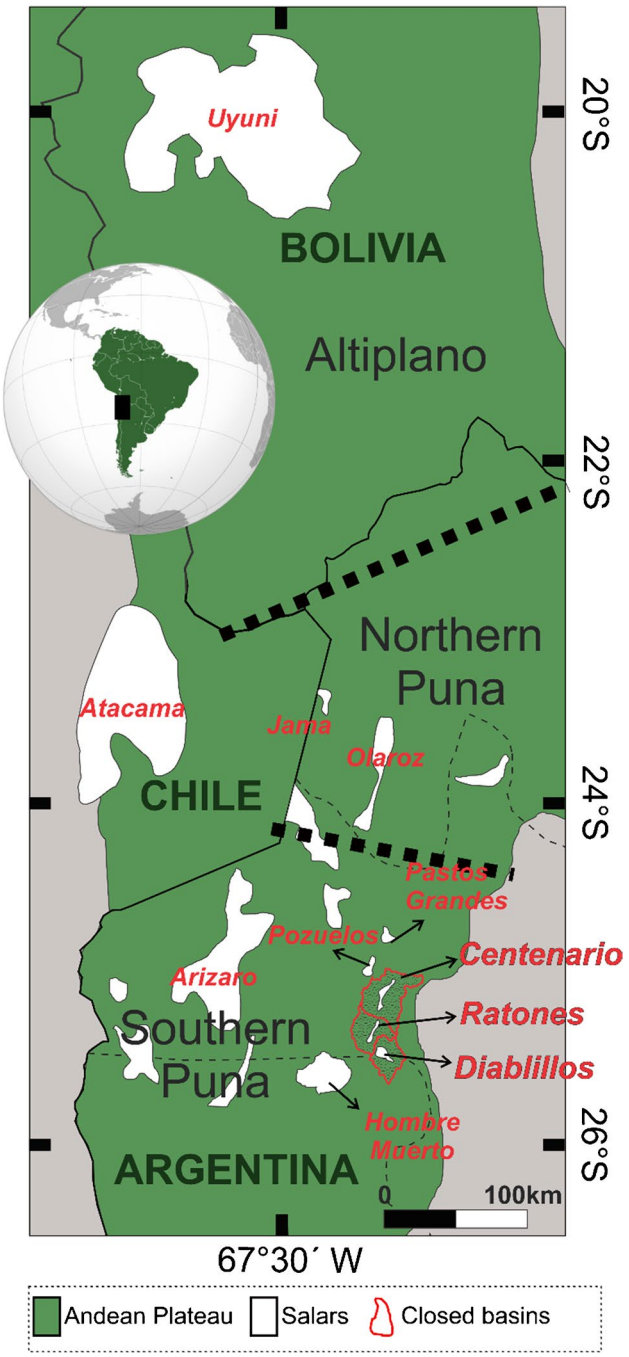

Fig. 1 Regional map of the Altiplano-Puna plateau modified after López Steinmetz et al. (2018). Continuous and thin dotted black lines represent international and provincial boundaries, respectively. Divisions within the Andean plateau (green area) are indicated with thick dashed lines, defining the Altiplano, Northern, and Southern Puna regions (Alonso et al. 1984). The southernmost division is represented by the Calama-Olacapato-Toro lineament (Alonso and Viramonte 1987; Allmendinger et al. 1997), which lies approximately at 24° S and divides the Puna geological province into the northern and southern part. Main salars in white. The study area includes the Diablillos, Centenario, and Ratones closed basins (solid red lines), see Fig. 2 for more details

to the deposition of various salts that accumulated mainly in the morphologically lowest parts of the salars.

The eastern boundary of the Diablillos, Ratones, and Centenario basins is represented by the Luracatao-Filo de Oire Grande Mountain Range, while the western boundary is mainly constituted by the Filo de Copalayo Mountain Range. The Diablillos basin is bounded and isolated from the Ratones basin by the Inca Viejo Range to the NW (Fig. 2). The Ratones basin is bordered by the Cerro Ratones hill (volcano) to the south, and the Centenario basin is bordered by the Pozuelos and Pastos Grandes basins to the north (Hains Engineering Company Limited 2018; Millennial Lithium 2019). The Centenario and Ratones basins are separated by the coalescence of alluvial fan deposits within the salar environment (Hongn and Seggiaro 2001). The Centenario depocenter is the largest (1005 km^2) followed by Ratones (593 km^2) and Diablillos (509 km^2) (Fig. 2), and the associated salars occupy an area of 7 km^2, 3 km^2, and 4 km^2, respectively (López Steinmetz et al. 2020). The Salar de Diablillos is at the highest altitude of 4000 m a.s.l; Ratones and Centenario are at 3820 and 3810 m a.s.l, respectively.

Lithology of the catchment area

The catchment areas of the three closed basins present quite different lithological units (Fig. 2). The catchment area of the Diablillos basin consists almost exclusively of Early Paleozoic metamorphic and magmatic basement rocks, which are subdivided in meta-sedimentary low- to medium-grade rocks (Rio Blanco Metamorphic Complex; Hongn and Seggiaro 2001) and Cambrian-Ordovician granitoids (Oire Eruptive Complex/OEC; Blasco and Zappettini 1996). The granitoids from the Luracatao and the Sierra del Inca Viejo ranges include peraluminous granites and granodiorites as well as orthogneiss. Cenozoic volcanic rocks are restricted and are represented by small outcrops of Miocene dacitic porphyries assigned to the Inca Viejo Formation (Hongn 1995).

The eastern part of the Ratones catchment also contains abundant Cambrian-Ordovician granitoids of the OEC. The western part of the catchment consists of Ordovician basement rocks such as pelite-greywacke meta-sedimentary rocks (with intercalated volcanic rocks) of the Falda Cienaga Formation (Aceñolaza et al. 1976). The Filo de Copalayo Range consists of Paleogene continental sequences of sandstone and conglomerate with volcaniclastic intercalations (Pozuelos and Catal formations; Alonso and Gutiérrez 1986; Hongn and Seggiaro 2001), Miocene-Pliocene volcanic deposits (dacites of the Bequeville Formation; Turner 1961), and Quaternary mafic andesite flows linked to fissures and monogenic centers (Incahuasi Formation; Hongn and Seggiaro 2001). Miocene-Pliocene volcanic deposits of Ratones andesite occur in the south of the basin (González 1984).

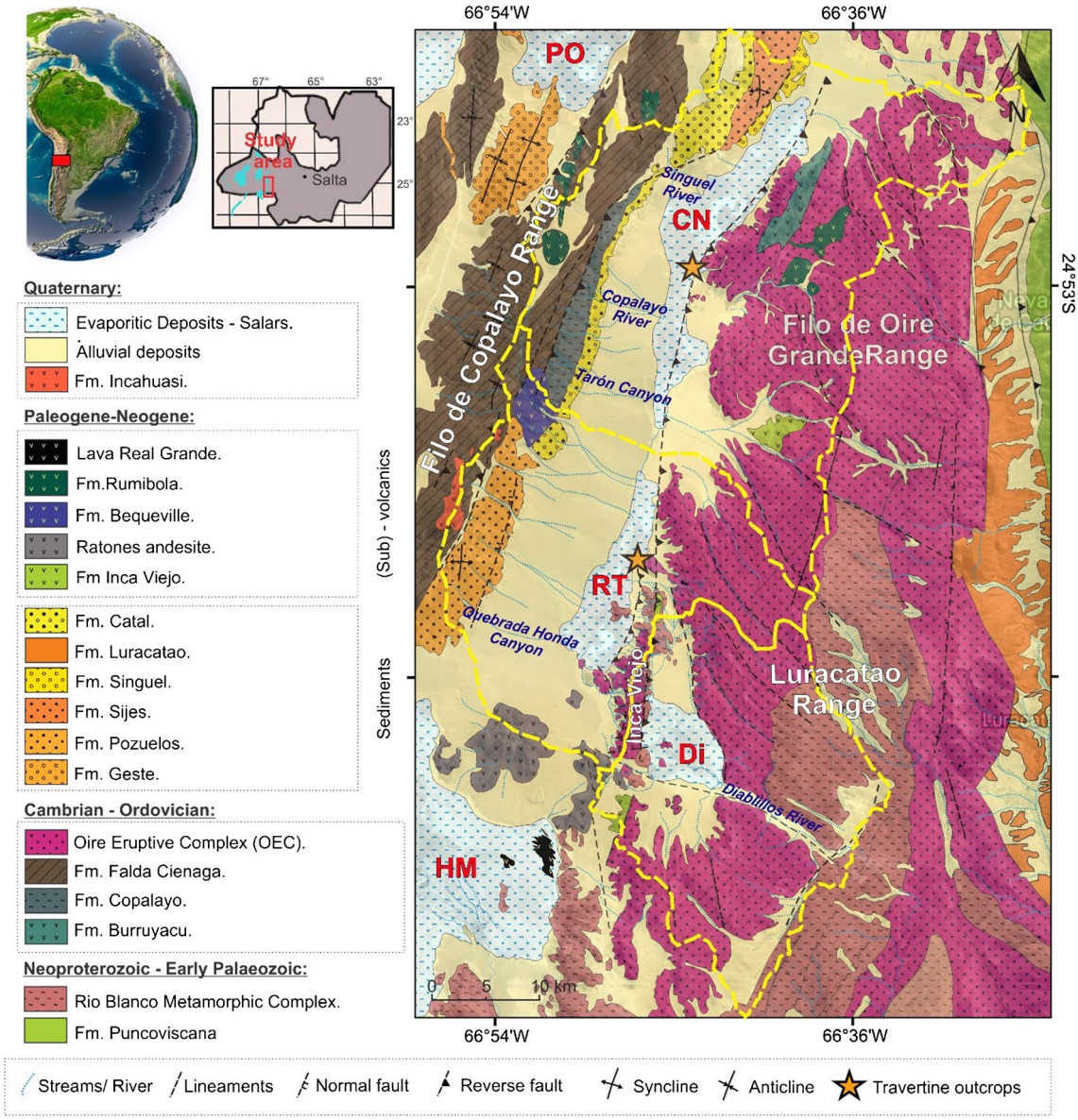

Fig. 2 Geological map of the study area based on Hongn and Seggiaro (2001), Blasco and Zappettini (1996), and Suzaño et al. (2015), with its location in northern Argentina. Closed basin limits of Diablillos (Di), Ratones (RT), and Centenario (CN) after Flo Solutions (2017), Hains Engineering Company Limited (2018), Millennial Lithium (2019), and Moran et al. (2019). PO and HM refers to Salar de Pozuelos and Salar de Hombre Muerto, respectively. Yellow stars refer to travertine outcrops

The Cambrian-Ordovician granitoids of the OEC and the low-grade Ordovician meta-dacites of the Burruyacu Formation (Blasco and Zappettini 1996) are largely exposed in the eastern catchment of the Centenario closed basin, and Ordovician meta-sedimentary rocks of the Falda Cienaga and Copalayo (Aceñolaza et al. 1976) formations are found in the Filo de Copalayo Range. Continental Paleogene deposits with volcanic intercalations of the Sijes, Singuel, and Catal formations cover the Early Paleozoic basement in the west of the basin. Contemporary with the deposition of the continental deposits of the Sijes Formation, intense volcanic-subvolcanic activity occurred in this section of the Puna, represented by the lower Miocene Inca Viejo dacitic porphyries and the Rumibola andesite of upper Miocene-Pliocene age with outcrops in the east and west of the basin. Quaternary siliciclastic sediments are deposited as alluvial fans in the catchment areas of the three basins (Hongn and Seggiaro 2001).

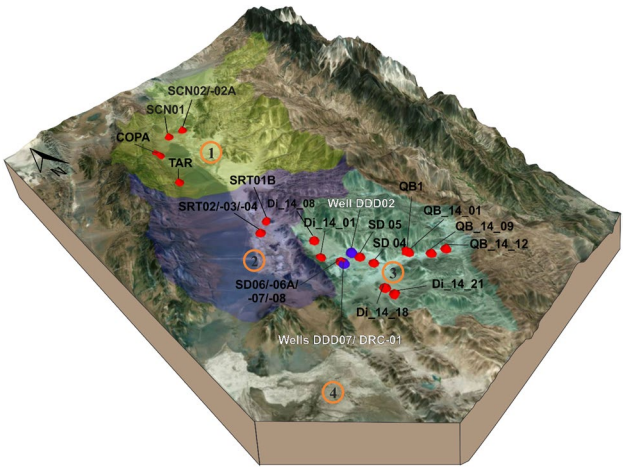

Fig. 3 Digital terrain model of the research area, indicating surface sampling sites (red cones) and Diablillos wells positions (violet cones). The green, purple, and light blue shadings schematically show the area covered by the Centenario, Ratones, and Diablillos closed basins, respectively. Numbers refer to the following salars: (1) Centenario, (2) Ratones, (3) Diablillos, and (4) Hombre Muerto

The salar basin deposits

All three salars correspond to the immature clastic salar type as classified by Houston et al. (2011) and have similar stratigraphic characteristics. The salars surface is characterized by a hard crystalline halite salt crust, which is better developed in the central part of the salars that transits outwards to more clastic facies. The stratigraphy comprises an upper layer (to a depth of 4 m) dominated by thin-bedded clay and silt deposits, with minor sands intercalated with borate deposits (mainly ulexite). Downwards, the infill continues with alternating siliciclastic sediments, represented by fine to medium sands with occasional coarser sands and gravels and very thin evaporite (mostly halite and less frequently gypsum) layers, till it reaches the Pz-basement rocks (at variable depths, SRK Consulting 2011; Flo Solutions 2017). Small, rounded borate concretions are most abundant in the Salar de Ratones and massive halite layers (up to 3 m) are most frequent in the Salar Centenario. Based on the description of a 252-m core from well DDD-07, a summary stratigraphic column of siliciclastic infill could be established for Salar de Diablillos (Fig. 4). Below the borate layer, alternating siliciclastic sediments (sandy layers interbedded with clays and silts) grade downward into coarser, gravel-dominated sediments overlying crystalline basement rocks, which occur at a depth of 240-m depth at the location of drill core DDD-07 (Fig. 4) and at 114-m depth at the location of monitoring well DDD-02 in the Salar de Diablillos (Rodinia Lithium 2011; Flo Solutions 2017). Basal conglomerates and breccias are deposited directly over the basement and largely consist of rock fragments derived from the underlying metamorphic rocks. This basement comprises fractured greenish phyllites and gneisses from the Rio Blanco metamorphic complex. The fractured basement functions as an aquitard with a low hydraulic conductivity of 0.01 m/day (Rodinia Lithium 2011). Basement rocks were recognized at 162 m in the Salar Centenario (own description). In the Salar de Ratones, two deep exploration drill holes performed by Eramine Sudamericana Company at the center and southern part of the salar encountered a thick basal ignimbrite deposit at 200-m depth (Rojas et al. 2019) and 70-m depth (126 m thick, own observation), respectively. These deposits have not yet been correlated to other ignimbrite deposits cropping out in the area. The brines of the salars are alkaline of the Na^+/Cl^--SO_4^{2-} type with pH values ranging between 7.5 and 8 (López Steinmetz et al. 2020). A distinctive feature of the Salar de Diablillos is high artesian conditions at depth and the presence of pressurized zones with high dissolved gas concentration of unknown origin in the aquifer. This is evidenced by the artesian behavior of some wells that intercept such pressurized areas and have been steadily producing without a pump.

The few ephemeral streams that feed the basins are mainly active during the rainy season in summer between January and March. Melting snow on the high eastern (Filo de Copalayo) and north-western (Luracatao and Filo de Oire Grande) foothills contributes to the precipitation input (Rodinia Lithium 2011). The Diablillos River is the only permanent tributary in the area and supplies the Diablillos basin with freshwater from the Luracatao Range throughout the year. Other drainage courses, that supply lower water flows, are the Singuel and Copalayo rivers, which drain into the Centenario basin from the eastern slope of the Filo de Copalayo Range (Fig. 2). No active hot springs have been identified in the study area, but in the south-east of Salar de Diablillos, along the Diablillos River, discontinuous travertine deposits have been described that are associated with former springs (Rodinia Lithium 2011) and are probably linked to the NW–SE orientated lineament that limits the south end of Salar de Diablillos. Discontinuous travertine deposits, which occur as 1- to 2-m thick relict terraces on the eastern side of the Centenario and Ratones salars, are associated with a regional N-S fault interpreted as the feeder of hot boron-bearing water (Alonso and Gutierrez 1984; Alonso and Viramonte 1987), bounding the eastern margin of the salars (Fig. 2).

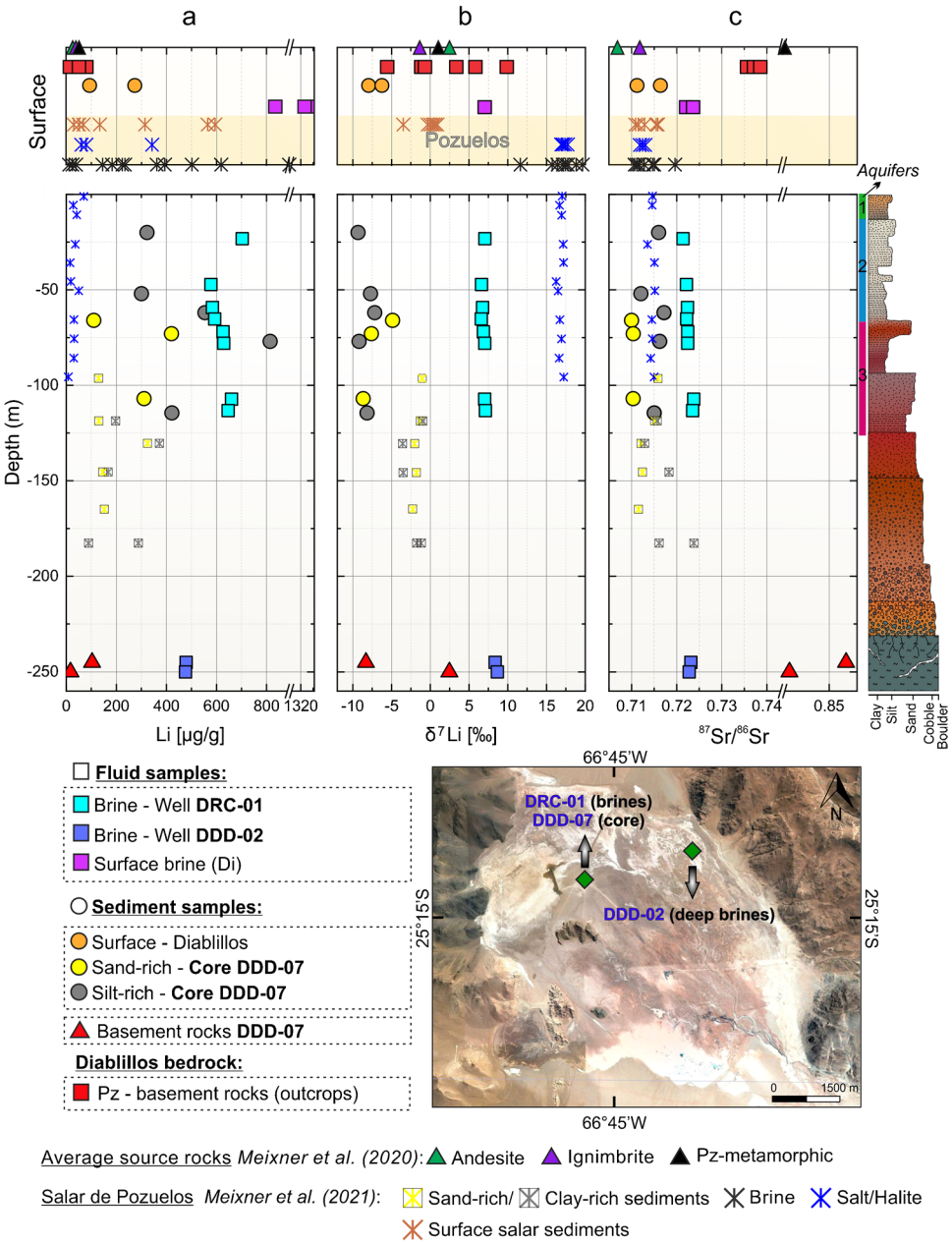

Fig. 4 Li concentrations, δ^7Li values, and $^{87}Sr/^{86}Sr$ ratios against sampling depth of surface samples and samples from wells DRC-01, DDD-02, and DDD-07 in Salar de Diablillos. The positions of the wells are also shown on the satellite image. The two basement brine samples from well DDD-02 are plotted together (at same depth) with the basement rocks from DDD-07 for interpretative purposes. The actual depth of the brine samples is given in Table 2. A schematic stratigraphic column of core DDD-07 from the nucleus of the salar is shown; green, blue, and pink stripes, to the left of the stratigraphic column, indicate aquifers 1, 2, and 3, respectively, as described in Diablillos Technical Report (SRK Consulting 2011). Average source rock data of the Central Andes are from Meixner et al. (2020). Salar de Pozuelos samples are presented for comparison (Meixner et al. 2021)

Materials and methods

Sample material

Catchment and basin surface samples

Catchment and basin surface samples include Pz-basement rocks, sediments, travertines, salt crusts, brines, and freshwater (Table 1). Samples from the Pz-basement include magmatic and low- to medium-grade metamorphic rocks from the Rio Blanco Metamorphic Complex ($n=5$) and rocks from the Oire Eruptive Complex ($n=2$) that comprise granitoids, orthogneisses, schists, and phyllites sampled at the Luracatao Range. Travertines ($n=2$) were sampled from the discontinuous terrace outcrops within Ratones and Centenario salars (Fig. 2). Samples of unconsolidated sediments ($n=4$) were collected from pits (30-cm depth) dug in the halite nucleus of all three salars. Brine samples ($n=6$) were taken from natural pools, mechanically dug exploration test pits, and from an artesian well. In some cases, surface brines and salt crust samples are collected as cogenetic pairs from natural pools in the Diablillos, Centenario, and Ratones salars (see Table 1 for pairs ID). Freshwater samples ($n=3$) are from the Diablillos River in the Diablillos basin and from the Copalayo River and Tarón Canyon in the Centenario catchment area. All near-surface salt crust, brine, sediment, and travertine samples were

Table 1 Li content and Li and Sr isotopic compositions of surface samples (sediments, brines, salts, fresh water, travertines, and Paleozoic metamorphic-magmatic basement rocks) from the Diablillos, Ratones, and Centenario salars and catchment areas. Nd isotope ratios are only available for sediment samples. Numbers in Pz-basement rocks refers to (1) Rio Blanco Metamorphic Complex and (2) Oire Eruptive Complex

	Description	Coordinates DMS	Pairs ID	Li (µg/g)	δ^7Li (‰)	2sd	^{87}Sr/^{86}Sr	2sd$_{mean}$	Sr (µg/g)	^{143}Nd/^{144}Nd	2sd$_{mean}$	εNd
Sediments												
SD04	Surface—Diablillos salar	25° 16′ 10.7″ S 66° 43′ 26.1″ W		89	−6.2	0.1	0.711294	0.000004		0.512285	0.000004	−6.9
SD07	Surface—Diablillos salar	25° 14′ 12″ S 66° 45′ 19.6″ W		272	−7.8	0.2	0.716461	0.000012		0.512261	0.000004	−7.4
SCN02	Surface—Centenario salar	24° 51′ 30.2″ S 66° 43′ 49.2″ W		69	−0.4	0.3	0.715146	0.000009		0.512266	0.000004	−7.3
SRT04	Surface—Ratones salar	25° 7′ 16″ S 66° 47′ 50.48″ W		40	−6.3	0.1	0.713396	0.000005		0.512261	0.000004	−7.4
*Brines**												
SD05	Artesian well—Diablillos nucleus	25° 14′ 58.8″ S 66° 43′ 46.6″ W		642	6.9	0.2	0.726680	0.000008				
SD06	Surface—Diablillos nucleus	25° 14′ 13.5″ S 66° 45′ 18.5″ W	1	1345	7.2	0.2	0.723833	0.000008				
SD07	Shallow pit in salar nucleus—Diablillos	25° 14′ 12″ S 66° 45′ 19.6″ W		837	7.1	0.2	0.722278	0.000008				
SD08	Surface—Diablillos nucleus	25° 14′ 30.7″ S 66° 45′ 19.6″ W		1327	7.1	0.1	0.723838	0.000006				
SCN02A	Surface—Centenario salar	24° 51′ 30.2″ S 66° 43′ 49.2″ W	2	852	9.2	0.2	0.715044	0.000010				
SRT03	Surface—Ratones salar	25° 7′ 15.06″ S 66° 47′ 49″ W	3	710	9.1	0.3	0.713335	0.000007				
Salt crusts												
SD06A	Salt from brine pool—Diablillos	25° 14′ 13.5″ S 66° 45′ 18.5″ W	1	174	6.9	0.2	0.723811	0.000005				
SD08	Surface—Diablillos nucleus	25° 14′ 30.7″ S 66° 45′ 19.6″ W		196	6.9	0.2	0.723833	0.000008				
SCN02A	Surface salt—Centenario salar	24° 51′ 30.2″ S 66° 43′ 49.2″ W	2	51	9.4	0.2	0.715401	0.000007				
SRT02	Surface salt—Ratones salar	25° 7′ 13.59″ S 66° 47′ 48″ W	3	61	8.8	0.2	0.713590	0.000008				
*Fresh water streams**												
QB1	Diablillos river (Diablillos)	25° 17′ 32″ S 66° 40′ 24″ W		11	5.4	0.1	0.715212	0.000006				
COPA	Copalayo river (Centenario)	24° 53′ 33″ S 66° 48′ 17″ W		5	5.1	0.2	0.713742	0.000005				
TAR	Tarón Canyon (Centenario)	24° 58′ 10″ S 66° 49′ 28″ W		1	6.3	0.3	0.735541	0.000007				
Travertines												
SCN01	Travertine—Centenario salar	24° 51′ 22.8″ S 66° 45′ 32.6″ W		77	3.7	0.2	0.715555	0.000006				
SRT01B	Travertine—Ratones salar	25° 06′ 40.3″ S 66° 46′ 26.2″ W		19	4.0	0.2	0.714215	0.000008				
Pz basement rocks												
QB-14–09	(1) Mica—schist	25° 18′ 53.52″ S 66° 39′ 9.30″ W		68	−5.5	0.1	0.914280	0.000011	22			
QB-14–12	(1) Mica—schist	25° 19′ 30.06″ S 66° 37′ 55.50″ W		29	−1.4	0.2	0.735707	0.000005	140			
QB-14–01	(2) Orthogneis	25° 17′ 16.13" S 66° 40′ 31.93" W		34	−0.6	0.2	0.737022	0.000008	128			
Di-14–21	(1) Schist—Tourmaline rich	25° 19′ 18.30″ S 66° 44′ 58.38″ W		79	9.7	0.1	1.122173	0.000016	23			
Di-14–18	(2) Granite	25° 18′ 22.72″ S 66° 44′ 56.88″ W		14	−0.6	0.1	0.738525	0.000006				
Di-14–08	(1) Phyllite	25° 11′ 17.10″ S 66° 45′ 18.78″ W		17	5.7	0.1	0.780605	0.000007	48			
Di-14–01	(1) Metasandstone	25° 12′ 48.54″ S 66° 46′ 16.02″ W		46	3.3	0.2	0.772681	0.000007				

(1) Rio Blanco Metamorphic Complex, (2) Oire Eruptive Complex

*mg/L

collected in May 2020, while freshwater and rock samples were collected in November 2014.

Drill cores

Drill core samples include brines, sediments, and Pz-basement rocks from cores and wells to a depth of 250 m from Salar de Diablillos (Table 2). Between 2009 and 2015, Rodinia Lithium Company explored the Salar de Diablillos for K, B, and Li resources and carried out drilling programs using diamond drilling with core recovery (wells identified as DD) and reverse circulation drilling with cutting recovery (wells identified as RC) together with deep brine sampling. To evaluate variations in isotopic composition and content with depth, sediments ($n=8$, silt-rich and sand-rich samples) were collected from depths between 20 and 115 m, and basement samples ($n=2$, phyllites) from the Rio Blanco Metamorphic Complex were collected from 245- and 250-m depths from the core from well DDD-07 (Flo Solutions 2017; Fig. 4).The brines ($n=8$) from well DRC-01 were sampled between 22.5- and 114-m depth, and the brines ($n=2$) from well DDD-02 were sampled between 132- and 156-m depth in the fractured Pz-basement. Wells DDD-07 and DRC-01 are both located in the center of the salar, while DDD-02 is located on the margin of the Salar de Diablillos (Fig. 4), where the basement is encountered at shallower depths (about 114 m). Core DDD-07 was drilled and sampled in July 2011, while the deep brines from wells DRC-01 and DDD-02 were collected in July 2010 and July 2011, respectively (Flo Solutions 2017).

Sample preparation and isotope analysis

Li concentration, stable isotopes of Li, and radiogenic isotopes of Sr and Nd were analyzed at the Isotope Geochemistry Laboratory at MARUM-Centre for Marine Environmental Sciences, University of Bremen, following the methods described in Meixner et al. (2020, 2021). Lithium isotope ratios are reported as δ^7Li values relative to the reference material NIST 8545. The repeatability of the individual δ^7Li values is given as two standard deviations; analytical uncertainty for Li concentrations is < 6% (2 sd). The analytical uncertainty for the radiogenic isotope ratios is given as $2sd_{mean}$. Details on sample preparation, analytical procedures, and reference materials are provided in the supplement ESM1.

Results

The elemental and isotope data are listed in Tables 1 and 2, and are also available through the World Data Center Pangaea (https://doi.pangaea.de/10.1594/PANGAEA.954690).

Surface samples

In the Salar de Diablillos, the brines ($n=4$) have Li concentrations ranging from 642 to 1345 mg/L and δ^7Li values from + 6.9 to + 7.2‰, while the corresponding values of the freshwater sample are 11 mg/L and + 5.4‰. The $^{87}Sr/^{86}Sr$ values of the brines are quite comparable (0.7223 and 0.7267) but differ significantly from the river sample (0.7152). The Li contents (174 and 196 µg/g) of two salt crusts from the center of the salar are significantly lower than those of the brines, while the isotope compositions of Li and Sr (+ 6.9‰ and 0.7238) are similar to the values of the brines. Two siliciclastic sediment samples from shallow pits in the center of the Salar de Diablillos have Li contents of 89 and 272 µg/g and δ^7Li values of − 7.8 and − 6.2‰. The Sr and Nd isotope compositions of the two sediment samples are comparable, averaging 0.7139 and 0.5123, respectively.

The brine sample from Salar de Ratones has a Li concentration similar to the lower range of the Diablillos samples (710 mg/L), but a higher δ^7Li value (+ 9.1‰) and a less radiogenic Sr isotopic composition (0.7133). The salt crust sample has a δ^7Li value of + 8.8 ‰ and an $^{87}Sr/^{86}Sr$ ratio of 0.7136 and closely resembles the isotopic composition of the cogenetic brine but has a lower Li content (61 µg/g). The siliciclastic sediment sample differs from the Salar de Diablillos samples in having a lower Li content (40 µg/g) but has similar Li, Sr, and Nd isotope compositions of − 6.3‰, 0.7134, and 0.5123. The travertine sample has a Li content of 19 µg/g with a Li isotope composition of + 4‰ and an $^{87}Sr/^{86}Sr$ ratio of 0.7142.

The Li content (852 mg/L), δ^7Li value (+ 9.3‰), and Sr isotope composition (0.715) of the brine sample and salt crust (51 µg/g; + 9.4‰; 0.7150) from Salar Centenario are similar to the composition of the brine and salt from Ratones. Two fresh-water samples have low Li concentrations (1 and 5 mg/L), positive δ^7Li values (+ 5.1 and + 6.3‰), and variable Sr isotope composition (0.7137 and 0.7355). The siliciclastic surface sediment sample has a Li content of 69 µg/g, a δ^7Li value of − 0.4‰, and an $^{87}Sr/^{86}Sr$ ratio of 0.7151, and has the same Nd isotope composition as the sediments from Diablillos and Ratones (0.5123). The travertine sample (Li content 77 µg/g; δ^7Li value + 3.7‰; $^{87}Sr/^{86}Sr$ 0.7156) has a similar composition to the travertine from Ratones.

In the catchment, Paleozoic basement rocks of the Rio Blanco Metamorphic Complex and Oire Eruptive Complex formations have Li contents ranging from 14 to 68 µg/g and δ^7Li values from − 5.5 to + 5.6‰ (with exception of a tourmaline-rich schist with 79 µg/g and + 9.6‰). The $^{87}Sr/^{86}Sr$ data range from 0.7370 to 1.1222 with most samples having ratios of 0.740 to 0.780.

Table 2 Li content and Li and Sr isotopic compositions of deep brines from wells DRC-01 and DDD-02, and core samples (sediments and basement rocks) from core DDD-07. For core samples, Nd isotope ratios are also given. Pz-basement rocks from core DDD-07 belong to (1): Rio Blanco Metamorphic Complex

	Description	Depth (m)	Li (µg/g)	δ^7Li (‰)	2sd	$^{87}Sr/^{86}Sr$	$2sd_{mean}$	$^{143}Nd/^{144}Nd$	$2sd_{mean}$	εNd
Sediments—Core DDD-07 (Salar nucleus) (25° 14′ 32.705″ S 66° 45′ 19.575″ W)										
CD_07_04	Sediment (silt-rich)	20	323	−9.3	0.2	0.716018	0.000007	0.512255	0.000004	−7.5
CD_07_10	Sediment (silt-rich)	52	300	−7.7	0.2	0.712083	0.000006	0.512314	0.000004	−6.3
CD_07_12	Sediment (silt-rich)	62	554	−7.2	0.2	0.717204	0.000006	0.512217	0.000004	−8.2
CD_07_15	Sediment (sand-rich)	66	110	−4.9	0.2	0.710015	0.000007	0.512371	0.000004	−5.2
CD_07_17	Sediment (sand-rich)	73	420	−7.6	0.2	0.710377	0.000006	0.512328	0.000004	−6.0
CD_07_19	Sediment (silt-rich)	77	814	−9.2	0.2	0.716245	0.000006	0.512273	0.000004	−7.1
CD_07_23	Sediment (sand-rich)	107	311	−8.7	0.2	0.710359	0.000006	0.512262	0.000007	−7.3
CD_07_24	Sediment (silt-rich)	115	422	−8.2	0.1	0.715041	0.000007	0.512251	0.000004	−7.5
CD_07_30	(1) Phyllite, Pz—basement (alterated)	245	103	−8.3	0.2	0.865160	0.000009	0.512152	0.000004	−9.5
CD_07_33	(1) Phyllite, Pz—basement (fresh)	250	17	2.5	0.1	0.814219	0.000007	0.512038	0.000004	−11.7
Brines—Well DRC-01 (Salar nucleus) (25° 14′ 32.705″ S 66° 45′19.575″ W)										
DRC01 #2	Deep brine	22.5–24	703	7.1	0.2	0.721408	0.000008			
DRC01 #6	Deep brine	46.5–48	578	6.6	0.2	0.722172	0.000006			
DRC01 #8	Deep brine	58.5–60	584	6.7	0.2	0.722411	0.000006			
DRC01 #9	Deep brine	64.5–66	593	6.6	0.2	0.722211	0.000006			
DRC01 #10	Deep brine	72	626	6.9	0.2	0.722463	0.000006			
DRC01 #11	Deep brine	78	629	7.0	0.2	0.722457	0.000006			
DRC01 #16	Deep brine	106.5–108	660	7.0	0.2	0.723780	0.000006			
DRC01 #17	Deep brine	112.5–114	647	7.1	0.2	0.723542	0.000006			
Brines—Well DDD-02 (Basement piezometer) (25° 14′ 16.215″ S 66° 43′ 57.693″ W)										
DDD02 #352	Deep basement brine	132–138	479	8.4	0.2	0.723152	0.000006			
DDD02 #356	Deep basement brine	150–156	477	8.7	0.2	0.722788	0.000005			

Drill core samples from Salar de Diablillos

In the core from well DDD-07, the Li contents and δ^7Li values of the sand-rich samples range from 110 to 420 µg/g and − 8.7 to − 4.9‰, while the isotopic compositions of Sr and Nd are 0.710 and 0.5123, respectively. For the silt-rich samples, values range from 300 to 814 µg/g, − 9.3 to − 7.2‰, 0.7121 to 0.7172, and 0.5122 to 0.5123, respectively. The unaltered/fresh basement rock has Li content, δ^7Li value, ^{87}Sr/^{86}Sr, and ^{143}Nd/^{144}Nd ratios of 17 µg/g, + 2.5 ‰, 0.8142, and 0.5120, respectively, while the altered rock has values of 103 µg/g, − 83‰, 0.8652, and 0.5122. Brine samples from well DRC-01, located in the center of the salar and collected from a subsurface sedimentary aquifer, have high Li contents ranging from 584 to 703 mg/L, Li isotope compositions ranging from + 6.6 to 7.1‰, and ^{87}Sr/^{86}Sr ratios ranging from 0.7214 to 0.7238. Two brine samples from well DDD-02 are from the deep fractured basement and have Li contents, δ^7Li values, and ^{87}Sr/^{86}Sr ratios of 477 and 479 mg/L, + 8.4 and + 8.7 ‰, and 0.7228 and 0.7232, respectively.

Discussion

We start this discussion by characterizing the bedrocks as potential sources for Li in the catchment and placing the siliciclastic sediments of the depocenters within the framework of catchment lithology and potential influence of intense Cenozoic magmatism using Sr and Nd isotope compositions (Fig. 5). Then we discuss the link between the Sr isotope composition of the Li bearing brine and potential rock sources of the catchments (Figs. 4c and 6a). The Li isotope fractionation by activation of the Li from potential host rocks (Cenozoic magmatic rocks, Pz basement) and secondary mineral formation in the sedimentary infill salar deposit is addressed using the Li isotope composition of source rocks, salar sediment, and brines and freshwater feeders (Figs. 4a; 6b). Finally, we locate the Centenario, Ratones, and Diablillos evaporitic Li deposits in the large picture of the Li province of the so-called Lithium-Triangle (Fig. 7, ESM2 Fig. A1).

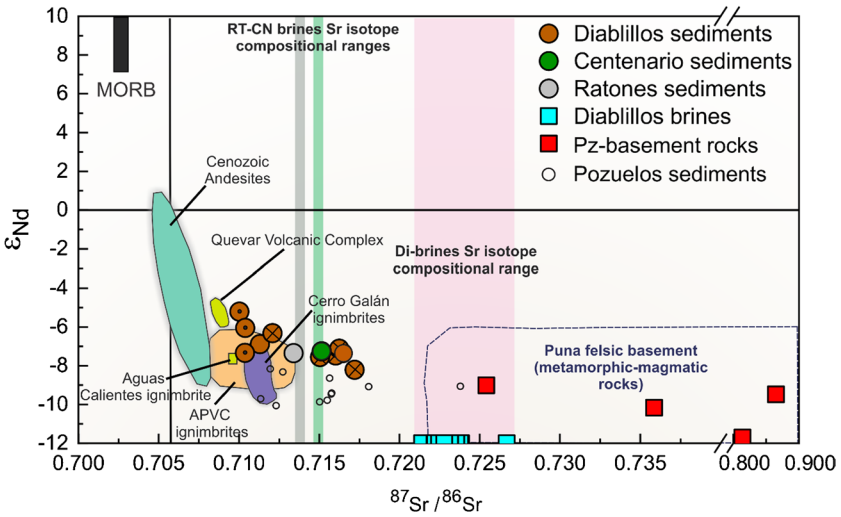

Fig. 5 ε_{Nd} values and ^{87}Sr/^{86}Sr ratios of sediments and brines from the Diablillos, Centenario, and Ratones salars. The colored circles indicate near-surface sediments from salars. Crossed brown circles are silt-rich sediments and circles with a dot in the center are sand-rich sediments from core DDD-07, Salar de Diablillos. With no Nd isotope data for the fluids, the pink, grey, and green vertical boxes indicate the ^{87}Sr/^{86}Sr range of the Diablillos, Ratones, and Centenario brines, respectively. The light blue squares indicate the ^{87}Sr/^{86}Sr ratios of the brines from the Diablillos drill core. Also plotted for comparison: average mantle composition (MORB, black bar) (Saunders et al. 1988), Cenozoic andesites (green field) (James 1982; Rogers and Hawkesworth 1989; Trumbull et al. 1999), Altiplano-Puna volcanic complex (APVC, orange field) ignimbrites (Lindsay 1999; Lindsay et al. 2001; Schmitt 1999), Cerro Galán ignimbrites (purple field) (Francis et al. 1989; Kay et al. 2011), andesites and dacites of the Quevar volcanic complex and Aguas Calientes Caldera ignimbrite (all yellow fields) (Matteini et al. 2002a, b) and Pz- felsic metarmorphic and magmatic basement rocks (field delimited by blue dashed line), and red square from Argentine lower Pz gneisses samples (Becchio et al. 1999; Lucassen et al. 2001). Neodymium isotopic composition is expressed with the ε_{Nd} notation, calculated using ^{143}Nd/.^{144}Nd CHUR = 0.512638 (Hamilton et al. 1983). Empty black circles correspond to Salar de Pozuelos surface and core sediment samples (Meixner et al. 2021)

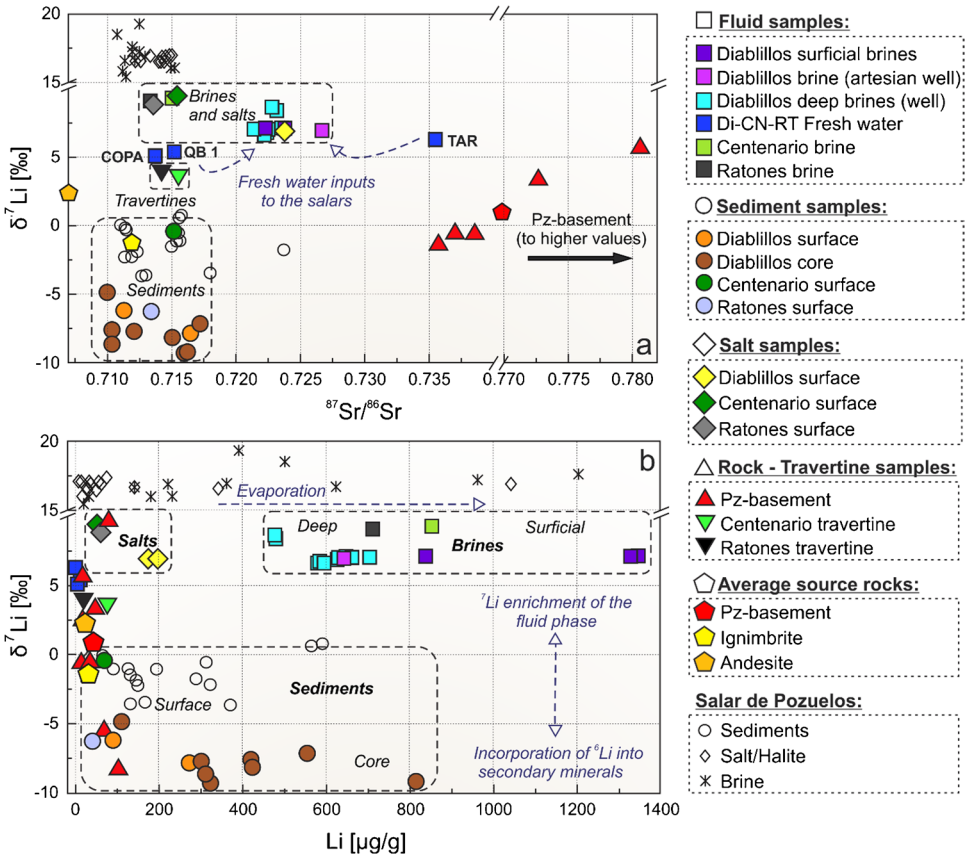

Fig. 6 δ^7Li values versus (**A**) ^{87}Sr/^{86}Sr ratios and versus (**B**) Li contents of fluids (fresh water and brines), sediments, salts, travertines, and bedrock samples from the Diablillos, Ratones, and Centenario closed basins. Brines and sediments recovered from wells and cores are differentiated from surface samples. In (**A**), four Pz-basement rocks with highly radiogenic ^{87}Sr/.^{86}Sr (> 0.782) are not shown (samples QB-14–09, Di-14–21, CD_07_30 and _33). The average Li and Sr isotope compositions of the Li source rocks are from Meixner et al. (2020), and the data for the samples from the Salar de Pozuelos are from Meixner et al. (2021)

Bedrock contributions to brine and sediment infill-Nd and Sr isotope evidence

Cenozoic volcanic and Paleozoic magmatic-metamorphic basement rocks have been proposed as the principal sources of lithium in the salars of the Altiplano-Puna plateau (Risacher and Fritz 2009; Hofstra et al. 2013; Meixner et al. 2020; López Steinmetz et al. 2020, among others). We discuss the composition of Diablillos, Centenario, and Ratones siliciclastic sediments, fluids (streams, rivers, brines), evaporites, and hydrothermal deposits (salt and travertine) in the framework of the different groups of source rocks based on their Sr isotope composition. The ^{87}Sr/^{86}Sr ratio imprinted on a fluid or sediment from its host or source changes only when mixed with different Sr isotopic compositions of other materials. The sources of siliciclastic sediments are also addressed by their radiogenic Nd isotopic (^{143}Nd/^{144}Nd) composition in the ε_{Nd} notation.

The Sr and Nd isotopic compositions of Cenozoic andesites, Cenozoic large volume ignimbrites, and Pz-basement plot within well-defined, distinct ranges on the regional scale of the high plateau (e.g., Meixner et al. 2020 and references therein). Metamorphic and magmatic Pz-basement rocks ($n = 7$, Fig. 2) of the Rio Blanco Metamorphic Complex and Oire Eruptive Complex are mostly felsic and show radiogenic ^{87}Sr/^{86}Sr, higher than 0.735 (Fig. 4c), similar to the compositional range of Pz-basement rocks—including Ordovician sedimentary rocks that were not analyzed in this study, but are present in the study area—reported on a regional scale by Meixner et al. 2020 (^{87}Sr/^{86}Sr average of 0.754). Outcrops of Cenozoic igneous rocks are scarce in all three catchment areas and have not been analyzed. Their uniform regional compositional ranges allow, however, the use of the published ranges. Compared to the Pz-basement, Cenozoic volcanic rocks have less radiogenic composition, with an average Sr isotope ratio of 0.707 ± 0.001 (2sd) for the andesite group and 0.710 ± 0.001 (2sd) for the large-volume ignimbrite of the Cenozoic magmatism (Meixner et al. 2020, and references therein) (Fig. 4c). The dominant Cenozoic volcanic rocks in the more distant vicinity of the basins are mainly the large-volume ignimbrites associated with the huge Cerro Galán Caldera to the south and the Aguas Calientes Caldera to the north. The ^{87}Sr/^{86}Sr ratios of Cerro Galán ignimbrites have whole-rock values mainly between 0.711 and 0.712 (Cerro Galán and Merihuaca ignimbrites, Real Grande dacite, Francis et al. 1989; Kay et al. 2011), and Aguas Calientes ignimbrite 0.709 ($n = 1$, Matteini et al. 2002a, b), both resembling the Sr isotope compositional ranges of this volcanism on the regional scale of the Altiplano-Puna plateau (Fig. 5; Mamani et al. 2010;

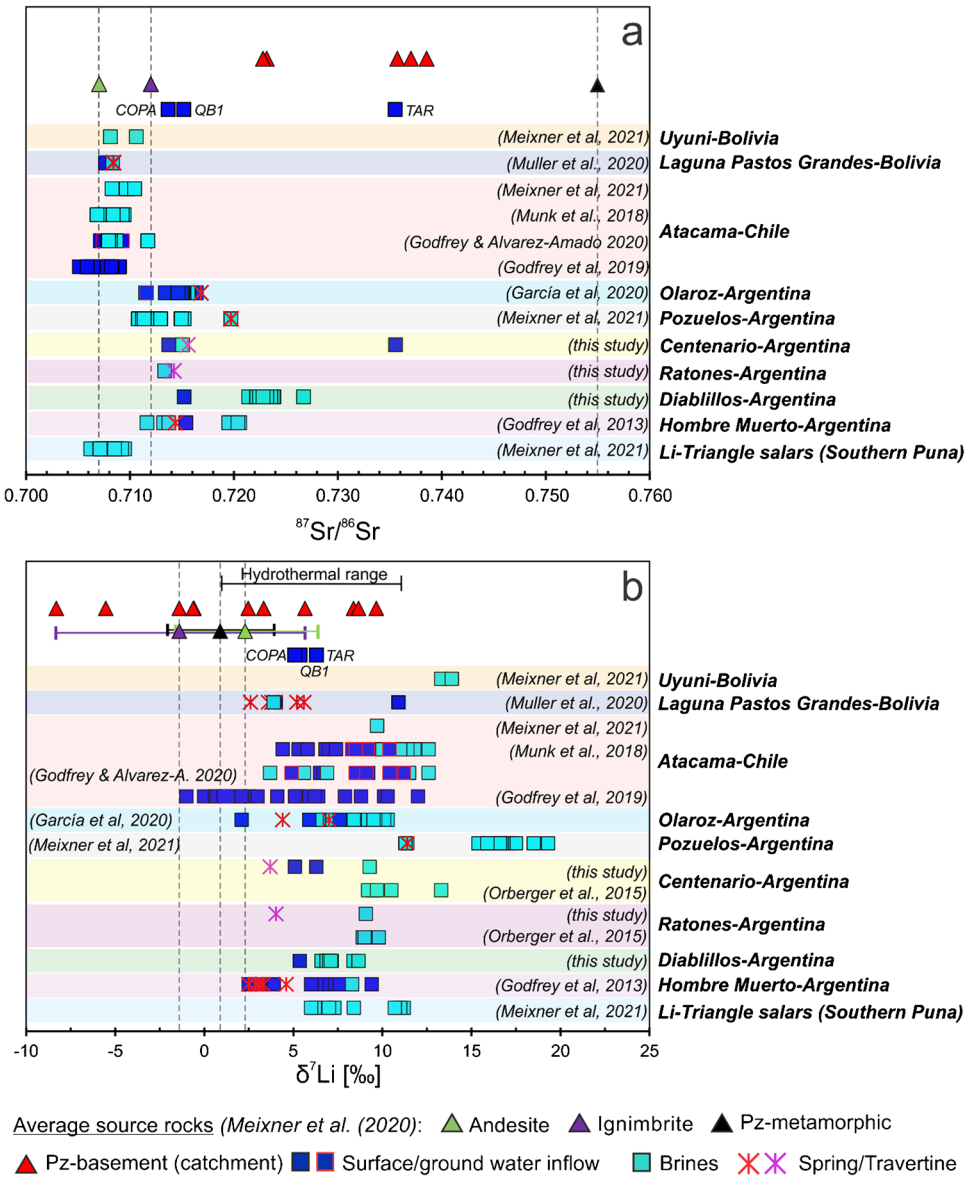

Fig. 7 A north to south compilation of Sr and Li isotope composition of salar deposits from the Lithium-Triangle in the Central Andes. (**A**) $^{87}Sr/^{86}Sr$ compositions of fresh water, brines, thermal waters, and sediments from different Altiplano-Puna salars (Meixner et al. 2021; Muller et al. 2020; Munk et al. 2018; Godfrey and Álvarez-Amado 2020; Godfrey et al. 2013, 2019; García et al. 2020; Orberger et al. 2015) together with $^{87}Sr/^{86}Sr$ values determined in different phases of Centenario, Ratones, and Diablillos salars. Average source rock compositions are from Meixner et al. (2020). (**B**) δ^7Li values for the same groups as in (**A**). The range of hydrothermal waters is from Pogge von Strandmann et al. (2016)

Kay et al. 2010; Brandmeier and Wörner 2016; Meixner et al. 2020).Considerable areas of the basins are also covered by widespread Cenozoic sedimentary deposits that recycle the local older rocks of the catchment and potentially store air-fall tephra and windblown dust material derived from pyroclastic rocks outside the catchment (see discussion in Meixner et al. 2021).

Siliciclastic sediments

The siliciclastic sediment in the depocentres of the basins should represent small, well-defined catchments with variable but generally steep morphological gradients of slope toward the depocenter. This means short distance transport of available detritus from physical weathering or other unconsolidated surface deposits in the catchment is expected. The siliciclastic surface sediments from the Ratones and Centenario depocentres have similar Sr (0.713 and 0.715) and Nd isotope signatures (ε_{Nd} −7.3 and −7.4) and fall within the isotope range of siliciclastic sediments (0.710 to 0.717; average 0.714 ± 0.006 (2sd), $n = 10$; ε_{Nd} ranges from −8.2 to −5.2) occurring at the surface and to depths of 115 m in the Diablillos depocentre. Thus, the sediments plot outside the compositional field of the abundant Pz-basement in the catchments, but also outside the Cenozoic andesite (Figs. 2 and 5). Instead, the Sr isotope composition of the siliciclastic sedimentary fill of the three salars is typical of Cenozoic large-volume silicic ignimbrites (Fig. 5). Cenozoic volcanic rocks do not dominate the surface geology of the catchments, and extensive silicic

ignimbrites are not even represented as outcrops in the area, but they cannot be strictly ruled out to dominate the sedimentary infill. It would be reasonable that pyroclastic material related to Cenozoic volcanism and/or sedimentary derivatives of pyroclastic rocks/tephra erosion might constitute an important component of the sedimentary material supplied to the salars infill. The presence of an important ignimbrite deposit buried in Salar de Ratones supports this assumption (Rojas et al. 2019), but this unit has so far not been mapped in the surface geology of the region nor correlated with any other known ignimbrite deposits in the region.

Despite the dominance of the Cenozoic volcanic signal in the Sr isotopic composition of the sediment fill, consistent differences in $^{87}Sr/^{86}Sr$ between coarser-grained, sand-rich samples with less radiogenic ignimbrite-type values and fine-grained, silt-rich samples with higher radiogenic values trending toward the Pz-basement are evident in core DDD-07 (Fig. 4c, Table 2). These differences can be linked to the different weathering responses (and transport) of the different source rocks in the catchment. Crystalline metamorphic and igneous rocks and well lithified Ordovician sedimentary rocks of the Pz-basement are expected to be less affected by physical weathering and more affected by in situ progressive chemical weathering, supplying solutes to the salar fluids (i.e., this is evidenced by the radiogenic compositions of Diablillos brines, see below). Contribution of detritus from the Pz-basement to the basin infill is most visible in the—compared to the composition of sand-rich samples—more radiogenic Sr isotope compositions of the silt-rich samples (Fig. 4c), most likely by addition of clay- to silt-size minerals from chemical weathering or small pristine detrital micas. In contrast, poorly indurated volcanic rocks and related poorly lithified pyroclastic material, already prone to chemical and physical weathering, can be easily washed into the basins' depocenters, dominating the coarser siliciclastic infill even in catchments dominated by the Pz-basement.

A quantification of the individual components is limited given the possible admixture of high $^{87}Sr/^{86}Sr$ micas from the Pz-basement. A simple binary mixing approach between an igneous-metamorphic Paleozoic basement endmember ($^{87}Sr/^{86}Sr$ of 0.74, Sr of 105 µg/g; Lucassen et al. 2001, and own data) and a Cenozoic large-volume silicic ignimbrite endmember (hereafter referred to as ignimbrite) ($^{87}Sr/^{86}Sr$ of 0.711, Sr of 270 µg/g; Kay et al. 2010; 2011) indicates that 60 to 100% of the Cenozoic ignimbrite (with a similar composition to the material erupted by the Cerro Galán Caldera) is needed to reach the Sr isotopic composition of the siliciclastic infill of the Diablillos, Centenario, and Ratones salars. This indicates that the siliciclastic sediments of these basins are dominated by debris from ignimbrite deposits and unconsolidated pyroclastic material eroded and redeposited by fluvial systems, together with easily transportable volcanic material supplied by neighboring eruptive centers in the back-arc as air-fall tephra deposits and windblown volcanic dust. The same situation was reported from the sedimentary column of the nearby Salar de Pozuelos basin (Figs. 2 and 4; Meixner et al. 2021).

Considering the presence of andesitic lavas and monogenetic centers, mainly in the Centenario and Ratones catchments, the Sr isotope composition of these salar sediments could also be modelled by mixing 30 to 60% of an andesite endmember (i.e., $^{87}Sr/^{86}Sr$ of 0.707, Sr of 530 µg/g; Meixner et al. 2020; Rosner et al. 2003 and references therein) with the Pz-basement composition. However, we favor the large-volume silicic ignimbrite as the dominant (although not exclusive) Cenozoic mixing component in the siliciclastic sediments of the Diablillos, Centenario, and Ratones salars deposits, considering that (1) Diablillos sediments plot together with Centenario and Ratones (and Pozuelos) samples, although the Diablillos (and Pozuelos) catchment present nearly no outcrops of Cenozoic volcanic rocks (Fig. 5), (2) strong differences in Sr isotope composition between sandy and mica-rich silty material of the sediment column are absent, i.e., a relatively high input of Pz-basement micas or clay should result in a higher radiogenic Sr isotope compositions in the silty sediment compared to the sandy sediments (Figs. 4 and 5, Table 2), and (3) Cenozoic large-volume ignimbrites, which form pyroclastic deposits that are easily transported by surface runoff and wind and are prone to alteration due to the large specific surface area of the porous material, dominate the wider area and occur in the Salar de Ratones section.

Freshwater, brines, and salts

The $^{87}Sr/^{86}Sr$ ratios of three local freshwater feeders range from 0.713 to 0.735. The unradiogenic $^{87}Sr/^{86}Sr$ of freshwater of the Copalayo River (COPA, 0.713), which drains into Salar Centenario, and the Diablillos River (QB1, 0.715), which feeds Salar de Diablillos (Figs. 2 and 6a), may be explained by the weathering of volcanic detritus. In the case of the Copalayo River, these materials may be associated with the presence of Cenozoic sedimentary deposits that crop out upstream in the Filo de Copalayo Range. No Cenozoic volcanic or sedimentary deposits are mapped for the Diablillos River catchment, which is fed by the Quebrada Barranquillas runoff. The radiogenic $^{87}Sr/^{86}Sr$ of the Tarón Canyon feeder (TAR, 0.735), which flows into the southern end of the Salar Centenario, relate to the low-grade Ordovician metasedimentary basement, i.e., the Falda Cienaga Formation, exposed in the Filo de Copalayo Range (Figs. 2 and 6a). The $^{87}Sr/^{86}Sr$ ratios (0.714 and 0.716) of two travertine deposits on the eastern margin of the Ratones and Centenario salars indicate that past hydrothermal activity

in the area appears to have sampled material with Sr isotope compositions near the regional average for Cenozoic ignimbrites (0.712, Meixner et al. 2020).

The brine and salt samples from the Salars de Diablillos, Centenario, and Ratones have very similar Sr isotopic compositions when sampled in pairs (Table 1) and can be divided in two distinct groups of Sr isotope compositions (Figs. 4c and 6a). The surface brines and salts of Centenario and Ratones range from 0.713 to 0.715 (average 0.714, $n=4$) and have compositions comparable to those of the siliciclastic sediments, the freshwater, and the travertine, and thus to those of the Cenozoic volcanic material, i.e., ignimbrites. The radiogenic Sr isotope signature of the freshwater from the Tarón Canyon seems to have no traceable influence on the $^{87}Sr/^{86}Sr$ of the brine in Centenario (Fig. 6a).

In contrast, the $^{87}Sr/^{86}Sr$ of the surface and deep brines and the salts from the Salar de Diablillos cluster in a small range from 0.721 to 0.726 (average 0.723 ± 0.002 2sd, $n=16$) and are thus more radiogenic than all material from Ratones and Centenario and all sediments associated with the salt and brines in the Salar de Diablillos or the freshwater (Figs. 4c and 6a). This suggests (1) a higher contribution of Sr from the Paleozoic crystalline rocks to the brines (and salts) than recorded in the siliciclastic sediments, and (2) a limited interchange of Sr between brines and host sediments in Diablillos.

The Sr isotope composition of the siliciclastic sedimentary record from the three salt pans indicates an important influx of volcanic material despite the abundance or even dominance of Pz-basement in the respective catchments The quantification of the volcanic material remains speculative as two compositional endmembers, the ignimbrite and andesite, and the mixture of volcanic material and Pz-basement, are all possible outcomes. The regional setting with widespread large-volume ignimbrite deposits from the Cerro Galán Caldera provides a potential source for debris eroded from volcanic units (lavas, pyroclastic deposits) in the past and ongoing deposition of windblown debris. The decoupling of brine $^{87}Sr/^{86}Sr$ from $^{87}Sr/^{86}Sr$ of the coexisting siliciclastic infill in Salar de Diablillos has interesting implications for our speculations: chemical weathering (liberation of element compounds into an aqueous solution) of the genuine in situ basement bedrocks is seen in the brine whereas the siliciclastic sediments are dominated by the volcanic debris that is transported as unconsolidated material at the surface by occasional water flux. For the Diablillos brines, only 25 to 40% of the large-volume ignimbrite (less for the andesite) endmember is needed to explain its $^{87}Sr/^{86}Sr$ compositional range. The uniformity of the Sr isotope composition of the brine with depth and the lack of exchange (equilibration) with the Sr of the sedimentary host rock is also underlined by the composition of basement brine samples pumped from metamorphic basement rocks (Table 2; Fig. 4c). Brine was homogenized over time to the dominant signature and confirms the connection between the different aquifers previously pointed out in this salar by SRK Consulting (2011) (indicated in Fig. 4). This potential homogenization is supported by the radiogenic $^{87}Sr/^{86}Sr$ ratio (0.726) in a brine from an artesian well in the Salar de Diablillos. The understanding of the hydrogeological model of the studied basins is not yet comprehensive. However, considering the presence of pressurized zones with a high concentration of dissolved gas in the aquifer, assumed to enter the salar via deep-seated faults through the basin floor, a significant amount of groundwater (radiogenic) could also enter the Diablillos basin through deep-seated structures, or represent the influence of inter-basin flow from adjacent basins (e.g., radiogenic $^{87}Sr/^{86}Sr$ values in brines from Salar del Hombre Muerto, Fig. 7a). The influence of this radiogenic water inflow would be less important (or absent) in the Centenario and Ratones salars.

Li isotope fractionation: from the catchment to the salar

Li isotopes are useful tracers of weathering processes, especially of silicate rocks. Unlike Sr, the isotope variations of Li in surface waters are less dependent on differences in lithology, and the main control over the Li isotope system is the balance between primary mineral dissolution and secondary mineral formation (Pogge von Strandmann et al. 2020 and references therein). During chemical weathering, ^{6}Li is preferentially retained by the secondary solid products (clay minerals and iron hydroxides), leading to lighter $\delta^{7}Li$ values compared to the source rocks, while the dissolved fraction (fluid phase) is enriched in ^{7}Li, gaining a heavy $\delta^{7}Li$ signature compared to the fresh rocks (Pistiner and Henderson 2003; Rudnick et al. 2004; Kısakürek et al. 2004; Huh et al. 2001; Vigier et al. 2008; Hindshaw et al. 2019). Congruent weathering instead produces no Li isotope fractionation and bulk dissolution of Li-bearing minerals which lead to the direct transfer of the $\delta^{7}Li$ composition of the source rocks to the fluids, releasing high Li contents (Dellinger et al. 2015, 2017; Kısakűreket al. 2005; Pogge von Strandmann et al. 2010). Modelled experimental $\Delta^{7}Li$ between clay and fluids ($\delta^{7}Li_{clay}$–$\delta^{7}Li_{fluid}$) was found to inversely correlate with temperature, as was expected from stable isotope fractionation theory. During clay mineral formation at low temperatures, $\Delta^{7}Li$ values under − 16.6‰ were obtained (20 °C; Hindshaw et al. 2019) reaching values of − 19‰ when temperatures were near 5 °C (Vigier et al. 2008). Previously reported $\Delta^{7}Li$ between residual solids and solutions from areas with similar characteristics as the Diablillos, Centenario, and Ratones closed basins (dry climate, high relief, cold temperatures) are within the range listed above ($\Delta^{7}Li$ − 17.8‰ for the

Donggi Cona lake in the Tibetan Plateau, Weynell et al. 2017; − 18.3‰ in the Salar de Pozuelos; Fig. 2, Meixner et al. 2021).

In active volcanic areas, such as the Central Andes, hydrothermal activity in and around the volcanic edifices is an important process. At higher temperature conditions, the ratio between primary rock dissolution and secondary mineral formation changes, leading to a lower fractionation and a lower δ^7Li (Pogge von Strandmann et al. 2016; Millot et al. 2010; Millot and Négrel 2007; Henchiri et al. 2014). Pogge von Strandmann et al. (2016) observed that the formation of secondary minerals is strongly limited in geothermal waters and proposed a hydrothermal compositional field with a δ^7Li range between > 0 and < 11‰. The δ^7Li of hydrothermal fluids and salar deposits from the Central Andes were found to fit this compositional range (García et al. 2020; Meixner et al. 2021).

Local Pz-basement that was sampled in the Diablillos catchment is also present in the two other studied basins. Its average δ^7Li composition of + 0.8‰ ± 4 (n = 6; four samples omitted with δ^7Li above + 5‰ or below − 5‰ that represent altered samples or exotic mineralogy) is close to the average δ^7Li values of the regional Pz-metamorphic and magmatic basement (+ 0.9 ± 3‰ 2sd; n = 15; Figs. 4b and 6; Meixner et al. 2020). The input of fallout tephra or debris eroded from volcanic units (e.g., ignimbrites or lavas) appears to be important for the Centenario, Ratones, and Diablillos salars. The regional Li isotope composition of the Cenozoic volcanism is − 1.4 ± 7‰ for large-volume ignimbrites and + 2.3 ± 4‰ for andesite (Figs. 4b and 6; Meixner et al. 2020).

Freshwater from small streams connects sections of the catchment to the brine. The δ^7Li of the two samples COPA and TAR from Centenario and the sample from Diablillos are quite similar (+ 5, + 6.3, and + 5.4‰) and higher than δ^7Li values of potential source rocks, i.e., indicate incongruent dissolution of the latter and enrichment of ^{7}Li in the fluid as also indicated by the δ^7Li of the respective brines (see below). However, Li contents (5, 1, and 11 µg/g) and ^{87}Sr/^{86}Sr (0.713, 0.735, and 0.715) are rather variable, and the Sr isotope compositions of TAR and Diablillos (QB1) are significantly different from the uniform composition of the respective brines. The discussion of these misfits' brine-freshwater is beyond the scope of the small data set on freshwater, and we consider these data as a local feature of sampling of small areas in the catchment (see also the discussion above).

An estimate of the δ^7Li values of possible hydrothermal additions via the composition of the two travertines in the Centenario and Ratones salars remains unclear. Both samples show similar δ^7Li values of + 3.7 and + 4.0‰, respectively (Fig. 6). Based on the experiments of Marriott et al. (2004), the δ^7Li composition of the (paleo)spring fluids that deposited the travertines can be inferred based on Li isotope fractionation resulting from precipitation of either aragonite (~ 11‰) or calcite (~ 4‰.). For the given δ^7Li value of travertine, the coexisting hydrothermal fluids could have a δ^7Li value of around + 14.8‰ or + 6.8‰, respectively. Observations from an active spring system in the Salar de Pozuelos (see Meixner et al. 2021) and travertine structures in the Salar de Hombre Muerto (Godfrey et al. 2013) point to original aragonite precipitation and hence to a hydrothermal δ^7Li value closer to + 14.8‰. The different Li contents (19 and 77 µg/g; Fig. 6b) of the travertine with virtually no Li isotopic variation could be due to different Li concentrations of the hydrothermal fluid (Hathorne and James 2006).

Brines and salts from the surface to the depth of Diablillos sedimentary infill have a strikingly uniform Li isotope composition (between + 6.6 and + 7.2‰), and even the deepest brine samples from the fractured Pz-basement have only a slightly higher δ^7Li values of + 8.4 and + 8.7‰ (Fig. 4b). The δ^7Li values of the surface brines and salts of Salar Centenario and Ratones are about 2‰ heavier than those of Diablillos (Fig. 6). The δ^7Li value of the Ratones brine sample (+ 9.1‰) fits the range reported by Orberger et al. (2015) (between + 8.9 and + 9.8‰), while the δ^7Li value of the Centenario brine sample (+ 9.2‰) is lower than previously reported values (+ 10.5 and + 13.3‰; Orberger et al. 2015). All samples show higher δ^7Li values than their potential source rocks, the Pz-basement and Cenozoic volcanic rocks (Fig. 6), pointing to enrichment of ^{7}Li in the brine. As previously observed in the Salar de Pozuelos (see Meixner et al. 2021) and in the Salar de Olaroz (García et al. 2020), isotope fractionation of Li during the evaporation process between brine and crystallizing halite is negligible and differences are within analytical uncertainty (Fig. 6, Table 1). The lithium content in the salt does not exceed 196 µg/g, while the coexisting brines reach up to 1345 µg/g, reflecting how halite crystallization contributes to the final Li concentration in the brines (Fig. 6b). Although salt crusts have relatively high Li contents (from 51 to 196 µg/g, n = 4) and Li + can substitute for Na + in halite, the relatively large difference in the ionic radius severely limits this cation substitution (Shannon 1976). It is most probable that Li is incorporated as brine inclusions trapped in the halite crystals (Godfrey et al. 2013) rather than in the mineral structure.

The Li elemental concentrations (between 110 and 814 µg/g; average 407 µg/g, n = 8) and δ^7Li values (between − 9.3 and − 4.9‰; average − 7.8‰, n = 8) of the Salar de Diablillos siliciclastic infill are not uniform with depth but there is no systematic covariation between Li contents and Li isotope composition, depth, or the systematic variations of ^{87}Sr/^{86}Sr in sand- (lower) and silt-richer (higher) samples (Fig. 4). Compared with the δ^7Li values and Li contents of the Paleozoic and Cenozoic source rocks (Meixner et al. 2020), the δ^7Li values and Li contents of the sedimentary infill indicate substantial

enrichment of ^{6}Li and substantially higher Li contents, at least 10 times higher than in the source rocks (Fig. 6a) and are consistent with a high abundance of secondary minerals from weathering of the source rocks.

The δ^{7}Li value (− 6.3‰) of the surface sediment sample from Salar de Ratones resembles the δ^{7}Li value of the Diablillos sediment samples, indicating alteration and secondary clay mineral formation were also important at Ratones. In contrast, the δ^{7}Li value (− 0.4‰) of the surface sediment sample from Centenario resembles the Li isotope composition of the source rocks (Paleozoic basement and Cenozoic volcanic rocks) and suggests this sample is mainly formed by rock fragments without major alteration or low amount of secondary minerals (Fig. 6b).

We consider the average δ^{7}Li value (− 7.5 ± 0.2‰, $n = 11$; except the Centenario sample) of the sediments from the salars as the best approximation to the composition of the stored secondary minerals ("residue") in the closed basins. This value is substantially lower than the average δ^{7}Li value (− 1.4‰ to + 2.3‰; Meixner et al. 2020) of the potential source rocks. Furthermore, the high average Li content of 407 µg/g exceeds the average contents in the different sources (about 20 to 40 µg/g; Meixner et al. 2020) and can be only related to the abundance of alteration products (clays) and masks the potential influence of admixing pristine material, i.e., we consider the δ^{7}Li of these sediments as close to the composition of altered rock. Considering the average brine (solution) compositions of + 7.2‰ (Diablillos) and + 9.3‰ and + 9.1‰ (Centenario and Ratones), respectively, as representing the average compositions of the aqueous solutions from weathering and hydrothermal activity, the apparent Li isotope fractionation ($\Delta^{7}Li_{residue\text{-}solution}$) is − 15‰, − 17‰, and − 17‰ for Diablillos, Centenario, and Ratones, respectively. The estimated Δ^{7}Li values for Centenario and Ratones salars are closer to the experimental average value of -16.6‰ determined by Hindshaw et al. (2019) between clay minerals and initial solution at low temperature conditions (20 °C) and smaller than the Δ^{7}Li calculated between brines and salar sediments in Salar de Pozuelos (− 18.3‰, Meixner et al. 2021), where mobilization of Li from the source rocks occurs mainly by near-surface (referred to as "low temperature") weathering. The lighter δ^{7}Li values registered in Diablillos brines (and salt) might reflect the input of fluids mainly from hydrothermal leaching or the occurrence of congruent weathering in the Diablillos catchment, both potentially limiting the degree of Li isotope fractionation between solid and solute. In addition, the δ^{7}Li values fit the hydrothermal compositional field proposed by Pogge von Strandmann et al. (2016) (ranging in between 1 and 11‰) and are close to the δ^{7}Li values of brines from the neighboring Salar del Hombre Muerto (+ 8.3‰), for which the weathering of volcanic deposits combined with significant influence of geothermal waters were proposed as the main mobilization processes (Godfrey et al. 2013).

Conclusions in the framework of current knowledge of Sr and Li isotopes in the Lithium-Triangle

The Sr isotope composition of different evaporite deposits (brine and salt; see Fig. 7a for references to locations) from the Altiplano-Puna region is largely consistent with the regional prevalence of Cenozoic volcanic rocks with distinct Sr isotope signatures, i.e., large volume ignimbrite (Olaroz, Pozuelos, Centenario, Ratones and Hombre Muerto) or andesite (Uyuni, Laguna Pastos Grandes, Atacama, and salars of the southern Puna). The Sr isotope signature of the sedimentary infill of Salar de Diablillos is also dominated by the large-volume ignimbrite signature, despite the dominance of the Pz-basement with radiogenic Sr isotope composition in the catchment. The same situation was also observed in Salar de Pozuelos further north (Meixner et al. 2021). This underlines the importance of volcanic material in the clastic sedimentation even in areas without volcanic edifices and massive volcanic deposits and dominant Pz-basement in the catchment of the closed basins. In turn, the exceptionally uniform Sr isotope composition of the brines in Diablillos in our data-set indicates a major contribution of radiogenic Sr from the Pz-basement, as expected from its abundance in the basin's catchment area (and also at depth, with a remarkable fractured aquifer at Salar de Diablillos). Curiously, the brines have a uniform Sr signature in Diablillos and did not equilibrate with the Sr signature of the sedimentary infill of the depocenter. Investigations of the sedimentary infill of the basins (drill holes) are currently limited to Diablillos and Pozuelos and certainly require more detailed attention concerning different groups of detritus (rock fragments, minerals), also with respect to their importance for the interpretation of the Li isotope composition.

The emerging amount of Li isotope data from fluids (and salts) in the Lithium-Triangle for the tracing of processes of Li transfer from silicate host rock to aqueous fluid with the final concentration of Li by evaporation of this fluid (summarized in Fig. 7b) shows the following main characteristics. All aqueous fluids from freshwater to brines (and related salts) show enrichment of ^{7}Li with respect to the potential host rocks, i.e., the formation of residual minerals, i.e., "clay," that enrich ^{6}Li during Li extraction by weathering or hydrothermal leaching (or at least mixing with high ^{7}Li fluids from such a process). The "end-member" of water–rock reaction, congruent solution of the

source rocks, is restricted to some ground water samples. The evaporation process and final precipitation of salt do not further fractionate the Li isotopes but enrich Li in the brine (summarized in ESM2 Fig. A1).

The siliciclastic sedimentary column (drill holes) in Diablillos and Pozuelos obviously samples Li with δ^7Li values isotopically lighter, i.e., enriched in ^{6}Li, compared to the δ^7Li values in the potential source rocks. Furthermore, average Li contents in the sediment column are enriched up to > 10 times the average value of ~ 40 µg/g in the large-volume ignimbrite, which has the highest average Li content among the three potential source rocks. The siliciclastic infill of the closed basins obviously stores residual minerals enriched in ^{6}Li throughout the stratigraphic column, i.e., as a continuous process in time. The calculated fractionation $\Delta^7Li_{residue\text{-}solution}$ considering the brine as the solution is close to values obtained from experiments and from similar natural settings in cold arid climate. A closer inspection of the components of the siliciclastic sediments could potentially reveal the location of the high Li contents and mixing relations between residue and pristine minerals. The δ^7Li values of the solutions (brines) are rather uniform in the respective basins and independent of the Li concentration.

Supplementary Information The online version contains supplementary material available at https://doi.org/10.1007/s00126-023-01181-z.

Acknowledgements The authors thank Geól. Walter Rojas, Eramine Sudamérica S.A., and PLASA (Potasio y Litio de Argentina S.A.) companies for the permission to perform Salar de Diablillos, Centenario, and Ratones sampling campaigns. We are also grateful to the late Paulino Cachizumba (IdGyM-UNJu) for sample preparation. C. Sarchi acknowledges doctoral fellowship from CONICET and Research Grants.

Funding Open Access funding enabled and organized by Projekt DEAL. This study is funded by CONICET and Research Grants—Short-Term Grants, 2019 (57440917) from the German Academic Exchange Service (DAAD) and supported by Project PIO UNJu-CONICET 14020140100010CO.

Declarations

Conflict of interest The authors declare no competing interests.

References

Aceñolaza FG, Durand F, Díaz Taddei R (1976) Geología y contenido paleontológico del basamento metamórfico de la región de Cachi, Provincia de Salta. Actas 5 Cong Geol Arg, 319–333.

Allmendinger RW, Jordan TE, Kay SM, Isacks BL (1997) The evolution of the Altiplano-Puna plateau of the Central Andes. Annu Rev Earth Planet Sci 25:139–174. https://doi.org/10.1146/annurev.earth.25.1.139

Alonso RN, Gutierrez R (1984) Zonación de ulexita en los salares de la Puna Argentina. Rev Asoc Geol Argent 34:52–57

Alonso RN, Viramonte JG (1987) Geología y Metalogenia de la Puna. Estud Geol 43:393–407

Alonso R, Gutiérrez R, Viramonte J (1984) Puna Austral - Bases para el sub-provincialismo geológico de la Puna Argentina. Abstr 9th Cong Geol Argentino 1:43–63

Alonso RN, Jordan TE, Tabbutt KT, Vandervoort DS (1991) Giant evaporite belts of the Neogene central Andes. Geology 19:401–404. https://doi.org/10.1130/0091-7613(1991)019%3c0401:GEBOTN%3e2.3.CO;2

Alonso RN, Gutiérrez R (1986) Litoestratigrafía del Neógeno terminal, Puna sudoriental argentina: Revista del Instituto de Geología y Minería de Jujuy 6:29-47

Bahlburg H, Berndt J (2016) Provenance from zircon U-Pb age distributions in crustally contaminated granitoids. Sediment Geol 336:161–170. https://doi.org/10.1016/j.sedgeo.2015.08.006

Becchio R, Lucassen F, Kasemann S, Franz G, Viramonte J (1999) Geoquímica y sistemática isotópica de rocas metamórficas del Paleozoico inferior. Noroeste de Argentina y Norte de Chile (21°–27° S). Acta Geol Hisp 34:273–299

Blasco G, Zappettini E (1996) Hoja geológica San Antonio de los Cobres, 2566–1, Programa Nacional de Cartas Geológicas, escala 1: 250.000. Boletín 217:126

Brandmeier M, Wörner G (2016) Compositional variations of ignimbrite magmas in the Central Andes over the past 26Ma — a multivariate statistical perspective. Lithos 262:713–728. https://doi.org/10.1016/j.lithos.2016.07.011

Büttner SH, Glodny J, Lucassen F, Wemmer K, Erdmann S, Handler R, Franz G (2005) Ordovician metamorphism and plutonism in the Sierra de Quilmes metamorphic complex: implications for the tectonic setting of the northern Sierras Pampeanas (NW Argentina). Lithos 83:143–181. https://doi.org/10.1016/j.lithos.2005.01.006

Chen C, Lee CTA, Tang M, Biddle K, Sun W (2020) Lithium systematics in global arc magmas and the importance of crustal thickening for lithium enrichment. Nat Commun 11(5):5313. https://doi.org/10.1038/s41467-020-19106-z

Dellinger M, Gaillardet J, Bouchez J, CalmelsD LP, Dosseto A, Gorge C, Alanoca L, Maurice L (2015) Riverine Li isotope fractionation in the Amazon River basin controlled by the weathering regimes. Geochim Cosmochim Acta 164:71–93. https://doi.org/10.1016/j.gca.2015.04.042

Dellinger M, Bouchez J, Gaillardet J, Faure L, Moureau J (2017) Tracing weathering regimes using the lithium isotope composition of detrital sediments. Geology 45:411–414. https://doi.org/10.1130/G38671.1

Flo Solutions (2017) Technical report resource estimate for lithium & potassium Sal de los Angeles project. Santiago.

Francis PW, Sparks RSJ, Hawkesworth CJ, Thorpe RS, Pyle DM, Tait SR, Mantovani MS, McDermott F (1989) Petrology and geochemistry of volcanic rocks of the Cerro Galan caldera, northwest Argentina. Geol Mag 126:515–547. https://doi.org/10.1017/S0016756800022834

Franco MG, Peralta Arnold YJ, Santamans CD, López Steinmetz RL, Tassi F, Venturi S, Jofré CB, Caffe PJ, Córdoba FE (2020) Chemical and isotopic features of Li-rich brines from the Salar

de Olaroz, Central Andes of NW Argentina. JS Am Earth Sci 103:102742. https://doi.org/10.1016/j.jsames.2020.102742

García MG, Borda LG, Godfrey L, López Steinmetz RL, Losada-Calderon A (2020) Characterization of lithium cycling in the Salar De Olaroz, Central Andes, using a geochemical and isotopic approach. Chem Geol 531:119340. https://doi.org/10.1016/j.chemgeo.2019.119340

Godfrey L, Álvarez-Amado F (2020) Volcanic and saline lithium inputs to the Salar de Atacama. Minerals 10(2):201. https://doi.org/10.3390/min10020201

Godfrey L, Chan LH, Alonso RN, Lowenstein TK, McDonough WF, Houston J, Li J, Bobst A, Jordan TE (2013) The role of climate in the accumulation of lithium-rich brine in the Central Andes. Appl Geochem 38:92–102. https://doi.org/10.1016/j.apgeochem.2013.09.002

Godfrey L, Herrera C, Gamboa C, Mathur R (2019) Chemical and isotopic evolution of groundwater through the active Andean arc of Northern Chile. Chem Geol 518:32–44. https://doi.org/10.1016/j.chemgeo.2019.04.011

González O (1984) Las ignimbritas «Ojo de Ratones» y sus relaciones regionales. Provincia de Salta. Actas 9 Cong Geol Arg. 206–220.

Goodenough JB (2016) Batteries and a Sustainable Modern Society. Interface Mag 25:67–70. https://doi.org/10.1149/2.f05163if

Grosjean C, Miranda PH, Perrin M, Poggi P (2012) Assessment of world lithium resources and consequences of their geographic distribution on the expected development of the electric vehicle industry. Renew Sustain Energy Rev 16:1735–1744. https://doi.org/10.1016/j.rser.2011.11.023

Hains Engineering Company Limited (2018) Mineral resource estimate & technical report on the Salar de Pozuelos project, Salta Province. Argentina, Toronto

Hamilton PJ, O'Nions RK, Bridgwater D, Nutman A (1983) Sm-Nd studies of Archaean metasediments and metavolcanics from West Greenland and their implications for the Earth's early history. Earth Planet Sci Letts 62:263–272. https://doi.org/10.1016/0012-821X(83)90089-4

Hathorne EC, James RH (2006) Temporal record of lithium in seawater: a tracer for silicate weathering? Earth Planet Sci Letts 246:393–406. https://doi.org/10.1016/j.epsl.2006.04.020

Henchiri S, Clergue C, Dellinger M, Gaillardet J, Louvat P, Bouchez J (2014) The Influence of hydrothermal activity on the Li Isotopic signature of rivers draining volcanic areas. Proc Earth Planet Sci 10:223–230. https://doi.org/10.1016/j.proeps.2014.08.026

Hindshaw RS, Tosca R, Goût TL, FarnanI TNJ, Tipper ET (2019) Experimental constraints on Li isotope fractionation during clay formation. Geochim Cosmochim Acta 250:219–237. https://doi.org/10.1016/j.gca.2019.02.015

Hofstra AH, Todorov TI, Mercer CN, Adams DT, Marsh EE (2013) Silicate melt inclusion evidence for extreme pre-eruptive enrichment and post-eruptive depletion of lithium in silicic volcanic rocks of the Western United States: implications for the origin of lithium-rich brines. Econ Geol 108:1691–1701. https://doi.org/10.2113/econgeo.108.7.1691

Hongn FD (1995) Zonas de cizalla precámbrico-paleozoicas y su vinculación con magmatismo cenozoico de posible interés económico. In Puna de Salta y Catamarca. Actas 5 Cong Nac Geol Econom, 264–280.

Hongn FD, Seggiaro RE (2001) Hoja Geológica 2566-III, Cachi, 1:250.000. Instituto de Geología y Recursos Minerales. Servicio Geológico Minero Argentino. Boletín 248 96.

Houston J, Butcher A, Ehren P, Evans K, Godfrey L (2011) The evaluation of brine prospects and the requirement for modifications to filing standards. Econ Geol 106:1225–1239. https://doi.org/10.2113/econgeo.106.7.1225

Huh Y, Chan LH, Edmond JM (2001) Lithium isotopes as a probe of weathering processes: Orinoco River. Earth Planet Sci Letts 194:189–199. https://doi.org/10.1016/S0012-821X(01)00523-4

Isacks BL (1988) Uplift of the Central Andean Plateau and bending of the Bolivian Orocline. J Geophys Res Solid Earth 93:3211–3231. https://doi.org/10.1029/JB093iB04p03211

James DE (1982) A combined O, Sr, Nd, and Pb isotopic and trace element study of crustal contamination in central Andean lavas, I. Local geochemical variations. Earth Planet Sci Letts 57:47–62. https://doi.org/10.1016/0012-821X(82)90172-8

Kay SM, Coira BL, Caffe PJ, Chen CH (2010) Regional chemical diversity, crustal and mantle sources and evolution of central Andean Puna plateau ignimbrites. J Vol Geoth Res 198:81–111. https://doi.org/10.1016/j.jvolgeores.2010.08.013

Kay SM, Coira B, Wörner G, Kay RW, Singer BS (2011) Geochemical, isotopic and single crystal $^{40}Ar/^{39}Ar$ age constraints on the evolution of the Cerro Galán ignimbrites. Bull Volcanol 73:1487–1511. https://doi.org/10.1007/s00445-010-0410-7

Kısakürek B, Widdowson M, James RH (2004) Behaviour of Li isotopes during continental weathering: the Bidar laterite profile, India. Chem Geol 212:27–44. https://doi.org/10.1016/j.chemgeo.2004.08.027

Kısakűrek B, James RH, Harris NBW (2005) Li and δ^7Li in Himalayan rivers: proxies for silicate weathering? Earth Planet Sci Letts 237:387–401. https://doi.org/10.1016/j.epsl.2005.07.019

Lindsay JM (1999) Stratigraphy, age relations and magmatic evolution of large-volume felsic ignimbrites of La Pacana Caldera, Central Andes, Chile. Univ Potsdam, Ph D thesis.

Lindsay JM, Schmitt AK, Trumbull RB, de Silva SL, Siebel W, Emmermann R (2001) Magmatic evolution of the La Pacana Caldera system, Central Andes, Chile: compositional variation of two cogenetic, large-volume felsic ignimbrites. J Petrol 42:459–486. https://doi.org/10.1093/petrology/42.3.459

López Steinmetz RL (2017) Lithium- and boron-bearing brines in the Central Andes: exploring hydrofacies on the eastern Puna plateau between 23° and 23° 30′ S. Miner Depos 52:35–50. https://doi.org/10.1007/s00126-016-0656-x

López Steinmetz RL, Salvi S (2021) Brine grades in Andean salars: when basin size matters. A review of the Lithium Triangle. Earth Sci Rev 217:103615. https://doi.org/10.1016/j.earscirev.2021.103615

López Steinmetz RL, Salvi S, García MG, Peralta Arnold Y, Béziat D, Franco G, Constantini O, Córdoba FE, Caffe PJ (2018) Northern Puna Plateau-scale survey of Li brine-type deposits in the Andes of NW Argentina. J Geochem Explor 190:26–38. https://doi.org/10.1016/j.gexplo.2018.02.013

López Steinmetz RL, Salvi S, Sarchi C, Santamans C, López Steinmetz LC (2020) Lithium and brine geochemistry in the Salars of the Southern Puna, Andean Plateau of Argentina. Econ Geol 115:1079–1096. https://doi.org/10.5382/econgeo.4754

Lucassen F, Becchio R, Harmon R, Kasemann S, Franz G, Trumbull R, Wilke HG, Romer RL, Dulski P (2001) Composition and density model of the continental crust at an active continental margin - The Central Andes between 21° and 27° S. Tectonophysics 341:195–223. https://doi.org/10.1016/S0040-1951(01)00188-3

Mamani M, Wörner G, Sempere T (2010) Geochemical variations in igneous rocks of the Central Andean orocline (13° S to 18° S): tracing crustal thickening and magma generation through time and space. GSA Bull 122:162–182. https://doi.org/10.1130/B26538.1

Marazuela MA, Ayora C, Vázquez-Suñé E, Olivella S, García-Gil A (2020) Hydrogeological constraints for the genesis of the extreme lithium enrichment in the Salar de Atacama (NE Chile): a thermohaline flow modelling approach. Sci Total Environ 739:139959. https://doi.org/10.1016/j.scitotenv.2020.139959

Marriott CS, Henderson GM, Crompton R, Staubwasser M, Shaw S (2004) Effect of mineralogy, salinity, and temperature on Li/Ca

and Li isotope composition of calcium carbonate. Chem Geol 212:5–15. https://doi.org/10.1016/j.chemgeo.2004.08.002

Matteini M, Mazzuoli R, Omarini R, Cas R, Maas R (2002a) The geochemical variations of the upper Cenozoic volcanism along the Calama–Olacapato–El Toro transversal fault system in central Andes (~24° S): petrogenetic and geodynamic implications. Tectonophysics 345:211–227. https://doi.org/10.1016/S0040-1951(01)00214-1

Matteini M, Mazzuoli R, Omarini R, Cas R, Maas R (2002b) Geodynamical evolution of Central Andes at 24° S as inferred by magma composition along the Calama–Olacapato–El Toro transversal volcanic belt. J Vol Geoth Res 118:205–228. https://doi.org/10.1016/S0377-0273(02)00257-3

Meixner A, Sarchi C, Lucassen F, Becchio R, Caffe PJ, Lindsay J, Rosner M, Kasemann SA (2020) Lithium concentrations and isotope signatures of Palaeozoic basement rocks and Cenozoic volcanic rocks from the Central Andean arc and back-arc. Miner Depos 55:1071–1084. https://doi.org/10.1007/s00126-019-00915-2

Meixner A, Alonso RN, Lucassen F, Korte L, Kasemann SA (2021) Lithium and Sr isotopic composition of salar deposits in the Central Andes across space and time: the Scalar de Pozuelos, Argentina. Miner Depos 57:255–278. https://doi.org/10.1007/s00126-021-01062-3

Millennial Lithium (2019) Feasibility study of the Pastos Grandes Project, Salta Province. Argentina, Santiago

Millot R, Négrel P (2007) Multi-isotopic tracing (δ^7Li, δ^{11}B, ^{87}Sr/^{86}Sr) and chemical geothermometry: evidence from hydro-geothermal systems in France. Chem Geol 244:664–678. https://doi.org/10.1016/j.chemgeo.2007.07.015

Millot R, Vigier N, Gaillardet J (2010) Behaviour of lithium and its isotopes during weathering in the Mackenzie Basin, Canada. Geochim Cosmochim Acta 74:3897–3912. https://doi.org/10.1016/j.gca.2010.04.025

Mon R, Hongn F (1987) Estructura del Ordovícico de la Puna. Rev Asoc Geol Argent 42(1–2):31–38

Mon R, Hongn F (1996) Estructura del basamento proterozoico y paleozoico inferior del norte argentino. Rev Asoc Geol Argent 51(1):1–10

Moran BJ, Boutt DF, Munk LA, Marconi P, Fisher JD, Arengo F, Frau D (2019) Revealing Paleo-groundwater and interbasin flow as fundamental to water and mineral resource sustainability on the arid Altiplano-Puna plateau. Abstr AGU Fall Meeting. San Francisco, H11N-1711.

Muller E, Gaucher EC, Durlet C, Moquet JS, Moreira M, Rouchon V, Louvat P, Bardoux G, Noirez S, Bougeault C, Vennin E, Gérard E, Chavez M, Virgone A, Ader M (2020) The origin of continental carbonates in Andean salars: a multi-tracer geochemical approach in Laguna Pastos Grandes (Bolivia). Geochim Cosmochim Acta 279:220–237. https://doi.org/10.1016/j.gca.2020.03.020

Munk LA, Hynek SA, Bradley D, Boutt DF, Labay K, Jochens H (2016) Lithium brines: a global perspective. Rev Econ Geol 18:339–365. https://doi.org/10.5382/Rev.18.14

Munk LA, Boutt DF, Hynek SA, Moran BJ (2018) Hydrogeochemical fluxes and processes contributing to the formation of lithium-enriched brines in a hyper-arid continental basin. Chem Geol 493:37–57. https://doi.org/10.1016/j.chemgeo.2018.05.013

Orberger B, Rojas W, Millot R, Flehoc C (2015) Stable isotopes (Li, O, H) combined with brine chemistry: powerful tracers for Li origins in salar deposits from the Puna Region, Argentina. Proc Earth Planet Sci 13:307–311. https://doi.org/10.1016/j.proeps.2015.07.072

Palmer MR, Edmond JM (1989) The strontium isotope budget of the modern ocean. Earth Planet Sci Letts 92:11–26. https://doi.org/10.1016/0012-821X(89)90017-4

Peralta Arnold Y, Cabassi J, Tassi F, Caffe PJ, Vaselli O (2017) Fluid geochemistry of a deep-seated geothermal resource in the Puna plateau (Jujuy Province, Argentina). J Vol Geoth Res 338:121–134. https://doi.org/10.1016/j.jvolgeores.2017.03.030

Pistiner JS, Henderson GM (2003) Lithium-isotope fractionation during continental weathering processes. Earth Planet Sci Letts 214:327–339. https://doi.org/10.1016/S0012-821X(03)00348-0

Pogge von Strandmann PAE, Burton KW, James RH, van Calsteren P, Gislason SR (2010) Assessing the role of climate on uranium and lithium isotope behaviour in rivers draining a basaltic terrain. Chem Geol 270:227–239. https://doi.org/10.1016/j.chemgeo.2009.12.002

Pogge von Strandmann PAE, Burton KW, Opfergelt S, Eiríksdóttir ES, Murphy MJ, Einarsson A, Gislason SR (2016) The effect of hydrothermal spring weathering processes and primary productivity on lithium isotopes: Lake Myvatn, Iceland. Chem Geol 445:4–13. https://doi.org/10.1016/j.chemgeo.2016.02.026

Pogge von Strandmann PAE, Kasemann SA, Wimpenny JB (2020) Lithium and lithium isotopes in Earth's surface cycles. Elements 16:253–258. https://doi.org/10.2138/gselements.16.4.253

Prezzi CB, Götze HJ, Schmidt S (2009) 3D density model of the Central Andes. Phys Earth Planet Inter 177:217–234. https://doi.org/10.1016/j.pepi.2009.09.004

Rapela CW, Pankhurst RJ, Casquet C, Dahlquist JA, Mark Fanning C, Baldo EG, Galindo C, Alasino PH, Ramacciotti CD, Verdecchia SO, Murra JA, Basei MAS (2018) A review of the Famatinian Ordovician magmatism in southern South America: evidence of lithosphere reworking and continental subduction in the early proto-Andean margin of Gondwana. Earth-Science Rev 187:259–285. https://doi.org/10.1016/j.earscirev.2018.10.006

Risacher F, Fritz B (2009) Origin of salts and brine evolution of Bolivian and Chilean salars. Aquat Geochem 15:123–157. https://doi.org/10.1007/s10498-008-9056-x

Risacher F, Alonso H, Salazar C (2003) The origin of brines and salts in Chilean salars: a hydrochemical review. Earth Sci Rev 63:249–293. https://doi.org/10.1016/S0012-8252(03)00037-0

Risacher F, Fritz B, Hauser A (2011) Origin of components in Chilean thermal waters. JS Am Earth Sci 31:153–170. https://doi.org/10.1016/j.jsames.2010.07.002

Rodinia Lithium (2011) NI 43–101 Technical report preliminary economic assessment Salar de Diablillos project Salta, Argentina.

Rogers G, Hawkesworth CJ (1989) A geochemical traverse across the North Chilean Andes: evidence for crust generation from the mantle wedge. Earth Planet Sci Letts 91:271–285. https://doi.org/10.1016/0012-821X(89)90003-4

Rojas W, Strecker M, Pingel H, Alonso R (2019) A Mio-Pliocene Li-bearing ignimbrite in the Ratones endorheic basin, Puna Plateau, Salta, Argentina. Abstr 15th Quadrennial IAGOD Meeting. p. 101.

Rosner M, Erzinger J, Franz G, Trumbull RB (2003) Slab-derived boron isotope signatures in arc volcanic rocks from the Central Andes and evidence for boron isotope fractionation during progressive slab dehydration. Geochem Geophys Geosyst 4. https://doi.org/10.1029/2002GC000438

Rudnick RL, Tomascak PB, Njo HB, Gardner LR (2004) Extreme lithium isotopic fractionation during continental weathering revealed in saprolites from South Carolina. Chem Geol 212:45–57. https://doi.org/10.1016/j.chemgeo.2004.08.008

Saunders AD, Norry MJ, Tarney J (1988) Origin of MORB and chemically-depleted mantle reservoirs: trace element constraints. J Petrol Special_Vol: 415–445. https://doi.org/10.1093/petrology/Special_Volume.1.415

Schmitt AK (1999) Melt generation and magma chamber processes in the Purico Complex and implications for ignimbrite formation in the Central Andes. Univ Potsdam. PhD thesis.

Shannon RD (1976) Revised effective ionic radii and systematic studies of interatomic distances in halides and chalcogenides. Acta Crystallogr Section A 32:751–767. https://doi.org/10.1107/S0567739476001551

SRK Consulting (2011) Preliminary economic assessment Salar de Diablillos project Salta, Argentina. NI 43–101 Technical Report.

Strecker MR, Alonso RN, Bookhagen B, Carrapa B, Hilley GE, Sobel ER, Trauth MH (2007) Tectonics and climate of the Southern Central Andes. Annu Rev Earth Planet Sci 35:747–787. https://doi.org/10.1146/annurev.earth.35.031306.140158

Suzaño NO, Becchio R, Sola A, Arnosio M, Nieves A (2015) Geología del prospecto Vicuña Muerta: emplazamiento múltiple y control estructural de cuerpos subvolcánicos Miocenos en el borde oriental de la Puna austral, Salta. Rev Asoc Geol Argent 72:519–541

Trumbull RB, Wittenbrink R, Hahne K, Emmermann R, Büsch W, Gerstenberger H, Siebel W (1999) Evidence for Late Miocene to recent contamination of arc andesites by crustal melts in the Chilean Andes (25–26°S) and its geodynamic implications. J South Am Earth Sci 12:135–155. https://doi.org/10.1016/S0895-9811(99)00011-5

Turner JC (1961) Estratigrafía del Nevado de Cachi y adyacencias. Acta Geológica Lilloana 3:191–226

Turner JCM (1970) The Andes of Northwestern Argentina. Geol Rundsch 59:1028–1063

Vandervoort DS, Jordan TE, Zeitler PK, Alonso RN (1995) Chronology of internal drainage development and uplift, southern Puna plateau, Argentine central Andes. Geology 23:145–148. https://doi.org/10.1130/0091-7613(1995)023%3c0145:COIDDA%3e2.3.CO;2

Vigier N, Decarreau A, Millot R, Carignan J, Petit S, France-Lanord C (2008) Quantifying Li isotope fractionation during smectite formation and implications for the Li cycle. Geochim Cosmochim Acta 72:780–792. https://doi.org/10.1016/j.gca.2007.11.011

Weynell M, Wiechert U, Schuessler JA (2017) Lithium isotopes and implications on chemical weathering in the catchment of Lake Donggi Cona, northeastern Tibetan Plateau. Geochim Cosmochim Acta 213:155–177. https://doi.org/10.1016/j.gca.2017.06.026

Willner AP, Gerdes A, Massonne HJ (2008) History of crustal growth and recycling at the Pacific convergent margin of South America at latitudes 29°–36° S revealed by a U-Pb and Lu–Hf isotope study of detrital zircon from late Paleozoic accretionary systems. Chem Geol 253:114–129. https://doi.org/10.1016/j.chemgeo.2008.04.016